hox13 genes are required for mesoderm formation and axis elongation during early zebrafish development

Zhi Ye and David Kimelman*
Department of Biochemistry
University of Washington
Seattle, WA 98195-7350

*Author for correspondence (kimelman@uw.edu)

Keywords: *hox* genes, *brachyury*, Wnt signaling, Neuromesodermal progenitors

Abstract

The early vertebrate embryo extends from anterior to posterior due to the addition of neural and mesodermal cells from a neuromesodermal progenitor (NMp) population located at the most posterior end of the embryo. In order to produce mesoderm throughout this time, the NMps produce their own niche, which is high in Wnt and low in retinoic acid. Using a loss of function approach, we demonstrate here that the two most abundant *hox13* genes in zebrafish have a novel role in providing robustness to the NMp niche by working in concert with the niche-establishing factor Brachyury to allow mesoderm formation. Mutants lacking both *hoxa13b* and *hoxd13a* in combination with reduced Brachyury activity have synergistic posterior body defects, in the strongest case producing embryos with severe mesodermal defects that phenocopy *brachyury* null mutants. Our results provide a new way of understanding the essential role of the *hox13* genes in early vertebrate development.

Summary Statement

The *hox13* genes are shown to have a novel critical role in ensuring development of the posterior body in zebrafish through sustaining the tailbud-derived bipotential neuromesodermal progenitors.

INTRODUCTION

A hallmark of early embryonic vertebrate development is the progressive formation of the posterior embryonic body from anterior to posterior (Kimelman and Martin, 2012; Steventon and Martinez Arias, 2017). This is clearly seen with the production of somites, which first form just behind the head and are then added sequentially until the final anterior-posterior (A-P) axis of the embryo is established (Holley, 2007; Pourquie, 2018). A key component of this process is a bipotential neuromesodermal cell progenitor (NMp) population located at the most posterior end of the embryo (the tailbud) during the somite-forming stages, which produces both the spinal cord and musculature (Gouti et al., 2015; Henrique et al., 2015; Kimelman, 2016b; Martin, 2016; Steventon and Martinez Arias, 2017; Wilson et al., 2009). The NMps express both the neural gene *sox2* and the mesodermal gene *T/Brachyury* (known as *tbxta* or *no tail* in zebrafish), allowing them to differentiate in either a neural or mesodermal direction. The canonical (β-catenin dependent) Wnt signaling pathway plays a key role in regulating this switch, such that NMps exposed to high Wnt enter the presomitic mesoderm and differentiate into various mesodermal fates such as muscle whereas those deprived of Wnt signaling become neural tissue. This mechanism allows the embryo to carefully balance the ratio of spinal cord to somites along the entire anterior-posterior axis, although in amniotes it occurs over a prolonged period whereas in anamniotes the fate decisions largely occur during gastrulation (Martin and Kimelman, 2012; Steventon and Martinez Arias, 2017).

What causes the termination of the embryonic A-P axis is uncertain. The simplest explanation is that the NMps, which progressively differentiate during the somitogenesis stages, are eventually depleted, resulting in the completion of the A-P axis. An intriguing alternative idea is that the most 5' *hox* genes (paralog group 13) actively terminate posterior extension along the A-P axis (Aires et al., 2019; Amin et al., 2016; Denans et al., 2015; Mallo, 2018; Steventon and Martinez Arias, 2017; Young et al., 2009). The initial impetus for this view came from the observation that knockout of the mouse *Hoxb13* gene caused the addition of two small somites at the tip of the tail, extending the embryo to 67 somites (Economides et al., 2003). Curiously, knockout of the other *Hox13* paralogs in mouse did not cause a lengthening of the body axis (Dolle et al., 1993; Fromental-Ramain et al., 1996; Godwin and Capecchi, 1998; Suemori and Noguchi, 2000).

Additional support for the proposed role of *hox13* genes in terminating the A-P axis in mouse came from experiments in which *Hoxa13*, *Hoxb13* and *Hoxc13* were overexpressed using a strong transcriptional promoter, resulting in embryos lacking all or most of the tail (Aires et al., 2019; Young et al., 2009). Additionally, chick embryos overexpressing *Hoxa13*, *Hoxb13* and *Hoxc13*, but not *Hoxd13*, showed slower ingression of mesodermal cells into the somites from the tailbud (Denans et al., 2015). Moreover, these authors showed that *Hoxa13* overexpression caused a reduction in the levels of the endogenous *T/Brachyury* gene, apparently through down-regulation of the Wnt signaling pathway. This leads to their proposal that a key job of the *Hox13* genes is to reduce the size of the presomitic mesoderm by progressively reducing canonical Wnt signaling.

A major caveat to the proposal that the *Hox13* genes limit the length of the A-P axis is that, with the one exception of the mouse *Hoxb13* mutant that causes a minor increase in the number of somites (as well as overgrowth of posterior neural tissue causing a wider and longer spinal cord), it is all based on overexpression studies. We chose instead to take a loss of function approach in zebrafish using CRISPR to mutate the two most abundant *hox13* genes in the tailbud. We show here that loss of *hoxa13b* or a combined loss of *hoxa13b* and *hoxd13a* does not cause posterior defects in an otherwise wildtype background. However, we show that *hoxa13b* and *hoxd13a* genes genetically interact with *tbxta*, the zebrafish ortholog of *T/Brachyury*, such that a combined reduction in Tbxta activity and loss of *hoxa13b* and *hoxd13a* leads to severe synergistic posterior embryonic defects. We show that these defects are due to a loss of mesoderm and a concomitant increase in *sox2* expressing cells, which parallels a sharp reduction in the expression of the posterior canonical *wnt* genes and the retinoic acid (RA)-degrading enzyme *cyp26a1,* as is observed in *tbxta* null mutants. Finally, using a newly created zebrafish line that overexpresses Hoxa13b we show that gain of function of Hox13 is not the opposite of loss of function, suggesting that *hox13* gene overexpression studies have the potential to be misleading. We propose that the *Hox13* genes' essential role is to provide robustness to the Brachyury-dependent NMp niche, which maintains Wnt signaling as well as preventing RA from accumulating in the tailbud, allowing the NMps to differentiate as mesoderm.

RESULTS

hoxa13b mutants are phenotypically normal

Zebrafish have six paralogs of the *hox13* cluster: *hoxa13a*, *hoxa13b*, *hoxb13a*, *hoxc13a*, *hoxc13b* and *hoxd13a*. Using data from a previous RNA-seq analysis of the tailbuds of mid-somitogenesis zebrafish embryos (Kimelman et al., 2017) we observed that all but *hoxb13a* are expressed at significant levels in the tailbud. We therefore made in situ hybridization probes to all the *hox13* genes except *hoxb13a* and observed that each of these is expressed in the tailbud at mid-somitogenesis as expected (Figure 1A). To determine the relative abundance of each of the *hox13* genes we used quantitative PCR, and found that *hoxa13b* and *hoxd13a* were the most abundant of the *hox13* genes and expressed at similar levels, with the remainder of the *hox13* genes expressed at lower levels (not shown).

Of the two most abundant *hox13* genes, we initially focused on *hoxa13b* since a previous overexpression study reported that *Hoxa13* inhibited mesodermal cell movements out of the chick tailbud whereas *Hoxd13* had no effect (Denans et al., 2015). *hoxa13b* is expressed in the future posterior mesoderm as early as the end of gastrulation, and continues to be expressed there until the end of somitogenesis (Figure 1B). The initial expression of *hoxa13b* at such an early stage of embryogenesis seemed surprising for a gene proposed to be involved in terminating axis formation. Therefore, we generated a mutant allele of *hoxa13b* that removes 16 bp in the middle of the coding region, eliminating the essential DNA binding region (Figure 2A). Embryos homozygous for *hoxa13b*$^{\Delta 16}$ were phenotypically completely normal, as were adults obtained from these embryos. One possibility for the lack of phenotype was compensation by the other *hox13* genes triggered by nonsense mediated decay, as has been observed in zebrafish for other transcripts with a premature termination codon (Ma et al., 2019). However, using qPCR we observed that the *hoxa13b*$^{\Delta 16}$ was expressed at the same level as wildtype *hoxa13b*, and that the other *hox13* genes were not upregulated in *hoxa13b*$^{\Delta 16}$ homozygous mutant embryos (not shown).

hoxa13b and *hoxa13b;d13a* mutants show posterior defects at lower temperatures

An alternate possibility for the lack of phenotype in *hoxa13b*$^{\Delta 16}$ embryos is that the other *hox13* genes are redundant with *hoxa13b*. We therefore mutated the other abundant *hox13* gene, *hoxd13a*, starting with adults that were homozygous for the *hoxa13b*$^{\Delta 16}$ mutation. Analysis of *hoxd13a* expression revealed that it also is activated early during somitogenesis,

starting at the 8-somite stage (Figure S1). We obtained three *hoxd13a* mutations, which inserted either 4 or 13 base pairs in the middle of the *hoxd13a* coding region, or deleted 8 base pairs at this site, with all of the mutations eliminating the DNA binding domain (Figure 2A). In crosses of heterozygous adults we observed embryos with a relatively low levels of tail defects from mild to severe (Figure 2B; crosses of *hoxa13b*$^{\Delta16/\Delta16}$;*hoxd13a*$^{ins13/+}$ fish produced 4.2% defective embryos, n = 188), with a very small number of these defective embryos surviving to adulthood (Figure S2). We observed a strong selection bias against double mutant females, but were able to obtain one double mutant female (*hoxa13b*$^{\Delta16/\Delta16}$;*hoxd13a*$^{ins4/ins4}$). Crossing this to a double mutant male of the same genotype produced 12.5% defective embryos (n = 40). These results demonstrate that *hoxa13b* and *hoxd13a* are redundant since posterior defects appear when both *hox13* genes are mutant.

In order to analyze the tail defects during the somitogenesis stages, we placed embryos from mutant crosses at 21°C beginning at the start of gastrulation (shield stage). We routinely use a post-shield stage cooling protocol since it allows us to examine embryos at all somitogenesis stages during the day after fertilization, rather than throughout the night as would occur if embryos were kept at the standard temperature of 28.5°C. As long as the embryos are cooled at shield stage or later, wildtype embryos develop completely normally at temperatures as low as 17°C (Kimelman, 2016a). When we performed this experiment on embryos from crosses of *hoxa13b*$^{\Delta16/\Delta16}$;*hoxd13a*$^{ins13+/-}$ adults, we surprisingly observed a range of posterior body defects from mild to severe. In order to quantify our results, we divided embryos into three classes of defects with the most severe embryos (class 1) appearing largely identical to embryos with a null mutation in *tbxta*, originally known as *no tail* (*ntl*) mutants (Halpern et al., 1993; Schulte-Merker et al., 1994, Figure 3A). Interestingly, however, unlike *ntl* mutants that have both a lack of tail and no notochord, our class 1 mutants all contained a notochord (Figure 3A). Crosses of *hoxa13b*$^{\Delta16/16}$;*hoxd13a*$^{ins13+/-}$ fish produced a range of embryos from classes 1 to 3 (Figure 3B, columns 1 and 2). We were able to identify *hoxa13b*$^{\Delta16/16}$;*hoxd13a*$^{ins13-/-}$ double homozygous mutant males, and these crossed to *hoxa13b*$^{\Delta16/16}$;*hoxd13a*$^{ins13+/-}$ females further enhanced the phenotype (Figure 3B, column 3). We similarly observed strong defects with crosses of *hoxa13b*$^{\Delta16/\Delta16}$;*d13a*$^{ins4+/-}$ and *hoxa13b*$^{\Delta16/\Delta16}$;*d13a*$^{\Delta8+/-}$ fish (Figure 3B columns 4 and 5). A cross of the one double homozygous female described above to a

double homozygous male, produced embryos that were virtually all class 1 and 2 (Figure 3B, column 6).

We next asked if the posterior defects were only found in *hoxa13b;d13a* double mutants, or if the same phenotype could be found in *hoxa13b* single mutants kept at 21°C. When we examined embryos from a cross of *hoxa13b*$^{\Delta 16/\Delta 16}$ fish we also observed posterior defects at 21°C, although at lower frequencies than with the *hoxa13b;d13a* mutants, and with half the embryos showing a wildtype phenotype (Figure 3C column 2 compared to 3B columns 1 and 2). Thus, removal of Hoxa13b function results in some posterior defects, but the effect is enhanced when Hoxd13a function is also reduced.

We previously reported that our wildtype stocks of zebrafish contain a naturally occurring variant of Tbxta containing two amino acid changes that leads to a cold-sensitive phenotype (Kimelman, 2016a). Embryos carrying this mutation, which we called *no tail*^{cs} (*ntl*^{cs}), have a completely wildtype phenotype when raised at the standard temperature of 28.5°C, but have the *ntl* null phenotype when raised at 17°C, including a lack of notochord. Since we were seeing cold-sensitive defects in our *hox* mutant fish we wondered if this mutation might also be present in our *hox* mutants, and therefore genotyped the fish described above. All of these fish were found to be homozygous for the *ntl*^{cs} mutation, suggesting that this contributes to the observed phenotype. When we raised homozygous *ntl*$^{cs/cs}$ embryos at 21°C we observed a minor number of posterior defects, but much less than was found in embryos that were also homozygous for *hoxa13b*$^{\Delta 16}$ (Figure 3C columns 1, 2). Similarly at 18.5°C, the absence of Hoxa13b function enhanced the *ntl*^{cs} phenotype (Figure 3C, columns 4 and 5). Stronger results were observed at both temperatures when fish that were homozygous for both *hoxa13b*$^{\Delta 16}$ and *ntl*^{cs} and heterozygous for *hoxd13a*^{ins13} were crossed (Figure 3C columns 3 and 6). Our results indicate that at 21°C and 18.5°C Tbxta function is only partially reduced in *ntl*^{cs} homozygous embryos, and that removal of Hoxa13b function enhances the strength of the posterior defect, which is further enhanced when Hoxd13a function is also depleted. However, the interaction between *tbxta* and the *hox13* genes is not likely due to an overall loss of Tbxta function, since the class 1 mutants appear very similar to *ntl* null mutants, yet have an intact notochord.

Hoxa13b;d13a mutants in a _ntl_ wt background are hypersensitive to Tbxta reduction

Since the above studies were done in a $ntl^{cs/cs}$ background we backcrossed our *hoxa13b;d13a* double mutant fish into a *ntl* wildtype background. These fish produced normal embryos at both 29°C and 18.5°C, demonstrating that it is a reduction in Tbxta function produced in ntl^{cs} embryos especially at lower temperatures that is necessary to cause posterior defects. To confirm that the reduction in Tbxta is the cause of the posterior defects, we injected wildtype and *hoxa13b;d13a* double mutant embyos in the *ntl* wildtype background with a very low dose (0.2 ng) of a *tbxta* morpholino oligonucleotide that we previously showed specifically phenocopies the *ntl* null mutation at 5 ng (Martin and Kimelman, 2008). We observed a marked hypersensitivity to reduced Tbxta levels when both *hoxa13b* and *hoxd13a* are mutated (Figure S3). These results further confirm the genetic interaction between the two *hox13* genes and *tbxta*.

Reduction of Tbxta and Hox13 function results in mesodermal deficits

To uncover the cause of the posterior phenotype defects, we examined gene expression using in situ hybridization on $hoxa13b^{\Delta 16\Delta J16};ntl^{cs/cs}$ embryos (hereafter called $hoxa13;ntl^{cs}$ embryos) placed at the semi-permissive temperature of 18.5°C from shield stage until mid-somitogenesis. We observed a sharp reduction in the expression of *tbxta* in the NMps in the majority of the $hoxa13;ntl^{cs}$ embryos, such that the only expression remaining at the most posterior end of the majority of embryos was the *tbxta* expression within the notochord progenitors, which are located just anterior to the NMps (Figure 4A, gray arrowhead; 53.3% of embryos showed a strong reduction in *tbxta*, n=30). The remaining embryos had less reduced or normal expression of *tbxta* (not shown). Interestingly, the expression of *tbxta* in the notochord (Figure 4A, black arrowhead) was normal in all of the $hoxa13;ntl^{cs}$ embryos, unlike in *tbxta/ntl* mutants where the expression of *tbxta* in the notochord is absent (Schulte-Merker et al., 1994 and see below). The normal *tbxta* expression in the notochord supports our observation that even class 1 embryos have an intact notochord (Figure 3A), and further supports the idea that the deficit in $hoxa13;ntl^{cs}$ embryos at the semi-permissive temperature is specific to the NMps and is not an overall loss of Tbxta function.

Since *tbxta* expression was strongly reduced, we examined other mesodermal markers including *tbx16* and *msgn1*, which mark the initial mesodermal progenitors (Fior et al., 2012; Griffin et al., 1998; Yabe and Takada, 2012), and *pcdh8*, which shows the presomitic mesoderm and nascent somites (Yamamoto et al., 1998). All of these genes were strongly downregulated in a majority of the *hoxa13;ntl*^{cs} embryos (Figure 4H-J; *tbx16*, 65.5%, n=27; *msgn1*, 63.2%, n=19, and *pcdh8*, 55.6%, n=27). Canonical Wnt signaling is essential both for *brachyury/tbxta* expression, and for the formation of the mesoderm, and so we examined the two posteriorly expressed canonical *wnt* genes, *wnt3a* and *wnt8a*. Both were strongly downregulated in *hoxa13;ntl*^{cs} embryos (Figure 4B,C; *wnt3a*, 89.7%, n=29; *wnt8a*, 90.3%, n=31). The same mesodermal defects were observed in class 1 *ntl*^{cs} homozygous embryos kept at 18.5°C that were wildtype for *hoxa13* and *hoxd13* (Figure S4), demonstrating that a loss of these two *hox13* genes synergistically enhances the effects of Tbxta reduction. Tailbud Wnt signaling is also regulated by two secreted Wnt inhibitors, Wif1 and Sfrp1a, which are expressed just anterior to the tailbud (Row and Kimelman, 2009). In *hoxa13;ntl*^{cs} embryos, expression of both genes was found to be closer to the posterior end of the embryo, further diminishing the levels of active Wnts (Figure S5). RA is kept out of the posterior end of the embryo by the Tbxta-regulated degrading enzyme, Cyp26a1, which is essential since RA blocks mesoderm formation (Martin and Kimelman, 2010; Olivera-Martinez et al., 2012; Sive et al., 1990). In *hoxa13;ntl*^{cs} embryos, *cyp26a1 was* also strongly downregulated (Figure 4D, 88.9%, n=27). These results indicate that the failure to form mesoderm is due to a loss of canonical Wnt signaling, together with an increase in RA in the posterior of the embryo due to a failure to sustain *cyp26a1* expression.

While the mesodermal genes were downregulated in *hoxa13;ntl*^{cs} embryos, not all posteriorly expressed genes were affected. For example, *cdx4* and *fgf8a* were normal or only partially reduced (Figure 4E,F; n=31 for *cdx4* and n=32 for *fgf8a*). Finally, we examined *sox2* since inhibition of Wnt signaling causes *sox2* to be expressed in the mesodermal region, which we also observed to varying degrees in *hoxa13;ntl*^{cs} embryos (Figure 4G; 84.6% with expanded *sox2* expression, n=26). The expansion of *sox2* into the mesodermal region is best seen with fluorescent in situ hybridization. In wildtype embryos, *sox2* expression is excluded from the mesodermal progenitors (Martin and Kimelman, 2012)(Figure S6A-C; Video S1). In *hoxa13;ntl*^{cs} embryos with a class 1 phenotype *sox2*

expands into this region, filling the entire posterior with *sox2*-positive cells (Figure S6D-F; Video S2). This is very similar to that observed in *tbxta/ntl* null mutants and morphants injected with the morpholino oligonucleotide that recapitulates the *ntl* mutant phenotype (Figure S6G-I; Video S3), except that in *hoxa13;ntl*^{cs} embryos the notochord is still present whereas in *tbxta/ntl* null mutants and morphants the notochord is absent (Figure S6E,H). We also observed the same expansion of neural fate in *hoxa13;ntl*^{cs} embryos with two other neural markers, *sox19a* and *pou5f3* (Figure S7). In summary, our results show a strong reduction of mesodermal gene expression and a concomitant increase in neural fated cells, exactly as shown for *tbxta/ntl* mutants (Martin and Kimelman, 2012) except that the notochord is unaffected, revealing that the absence of Hoxa13b enhances a reduction in Tbxta activity specifically within the NMps and their mesodermal derivatives.

The defect in *hoxa13;ntl*^{cs} mutant cells is rescued non-cell autonomously

Despite Tbxta having a large number of direct target genes (Garnett et al., 2009; Morley et al., 2009), we previously showed that individual *tbxta/ntl* mutant cells are rescued by the surrounding cells when transplanted into a wildtype environment (Martin and Kimelman, 2008). Thus, while *tbxta/ntl* mutants lack tail mesoderm, transplanted *tbxta/ntl* mutant cells contribute to tail mesoderm, demonstrating that the defect in *tbxta/ntl* is non-cell autonomous, which led to our proposal that the essential role of Brachyury/Tbxta is to control a small number of genes necessary to establish an NMp niche that has high Wnt and low RA, which is essential for mesoderm to form. To compare *hoxa13;ntl*^{cs} cells to *tbxta/ntl* mutant cells, we transplanted 30-50 dye-labeled cells at the start of gastrulation into the future posterior mesodermal region of the embryo, and then let the embryos develop for two days at the semi-permissive temperature of 18.5°C. For the *hoxa13;ntl*^{cs} mutants we only scored transplants in which the donor embryo, which was left to develop after the small number of cells used in transplantation were removed, developed as a class 1 or class 2 phenotype. Wildtype cells transplanted in this manner end up in the tail somites as expected (Figure 5A-C; n=18 host embryos scored). Similarly, *hoxa13;ntl*^{cs} cells also ended up in the tail somites, appearing indistinguishable from neighboring muscle cells (Figure 5D-F; n=96 host embryos scored). These results demonstrate that, exactly as with *tbxta/ntl* null cells (Martin and Kimelman, 2008), the defect in *hoxa13;ntl*^{cs} mutants is rescued by the surrounding cells. These results indicate that the absence of Hoxa13b enhances the defect

caused by decreased Tbxta function in the NMps, and does not produce additional cell autonomous differentiation defects.

Since overexpression analyses suggested a role for the *hox13* genes in cell movement (Denans et al., 2015; Payumo et al., 2016), we wished to compare cell movements in *hoxa13;ntl*^{cs} cells at the semi-permissive temperature to morphant cells lacking Tbxta. All embryos were injected with a nuclear EGFP then placed at 18.5°C at shield stage. At the 10s stage, *hoxa13;ntl*^{cs} embryos that showed a strong posterior phenotype, which will all go on to produce class 1 embryos, were identified and compared to wildtype and *tbxta* morphants by imaging on a confocal microscope. The speed and directionality of cell movements were analyzed as others have previously done for wildtype embryos (Das et al., 2019; Lawton et al., 2013; Mongera et al., 2018). Interestingly, the overall shape of the tailbud of *hoxa13;ntl*^{cs} embryos was the same as *tbxta* morphant tailbuds, and quite different from a wildtype tailbud (Figure 6F,I compared to C). To examine the movements in detail we examined both the NMps and mesodermal progenitor zone (MPZ), which is where *tbx16* and *msgn1* are first activated (Griffin et al., 1998; Yoo et al., 2003). In both regions, both the speed of movement and the "straightness" of movement are similarly reduced in both the *hoxa13;ntl*^{cs} embryos and *tbxta* morphants relative to wildtype embryos (Figure 6J-M). These results provide further support for the idea that a loss of *hoxa13b* enhances a partial reduction of Tbxta function within the NMps and mesodermal progenitors that derive from the NMps, producing defects that appear similar to a complete loss of Tbxta.

Overexpression of Hox13 proteins is not the opposite of loss of function

Since almost all of the previous studies involved overexpression analysis, we wished to examine the effects of conditionally overexpressing Hoxa13b and Hoxd13a in zebrafish. We produced two transgenic lines that express either Hoxa13b or Hoxd13a under the control of a heatshock promoter, which allows us to regulate the timing of transgene expression (*HS:hoxa13b* and *HS:hoxd13a*, respectively). mCherry was co-expressed with the Hox13 proteins in order to identify transgenic lines with strong expresion (Figure 7A). Prior to being heat shocked, embryos were allowed to develop until mid-somitogenesis (10s stage) to bypass any possible effects caused by prematurely producing the Hox13 proteins before the stages they are normally expressed. Whereas overexpression of Hoxa13b caused a severe posterior truncation, overexpression of Hoxd13a only caused defects in the

anterior of the embryo (Figure 7B). By quantitatively examining *mCherry* using qPCR, we observed that both transgenic lines produced similar levels of the co-expressed reporter, indicating that the differences were not likely due to differences in expression levels (Figure 7C). Interestingly, a study in chick examining cell movement defects caused by Hox13 overexpression found that Hoxa13 caused strong effects whereas Hoxd13 had no effect (Denans et al., 2015), showing that the effects of different Hox13 overexpression observed in amniotes are also seen in zebrafish.

Optimally, overexpression will cause the opposite effect of loss of function. However, overexpression of transcription factors is potentially problematic since it is possible that they could bind sites in the DNA when expressed at higher than endogenous levels that they would not normally bind when expressed at normal levels. Moreover, transcription factors are often in large protein complexes, and overexpression has the potential to create aberrant complexes or disrupt the normal stoichiometry of endogenous complexes. To analyze changes in gene expression caused by overexpression or loss of the Hox13 factors, we isolated tailbud explants from *hoxa13;ntl*^{cs} mutant embryos kept at 18.5°C, as well as tailbud explants from *HS:hoxa13b* embryos, three hours after a 10s heatshock, and examined the expression of a selection of genes. In both cases we cut the explants at the 15s stage, selecting for embryos that had a clear morphological defect since these will go on to produce embryos with strong posterior defects as shown in Figures 3A and 7B. In order to keep the anterior-posterior extent of the explants constant, they were all cut to extend from the most posterior end of the embryo to the third most newly formed somite.

In agreement with our in situ hybridization data, we observed decreased expression of *tbxta*, *msgn1*, *wnt3a*, *cyp26a1* and *tbx16* in the *hoxa13;ntl*^{cs} mutant embryos, with little to no effect on *cdx4* and *fgf8a* (Figure 7D). In embryos overexpressing Hoxa13b, we observed decreased expression in most of these genes, including *tbxta*, *wnt3a* and *wnt8a*. Importantly, decreased *T/Brachyury* expression was also observed with Hoxa13 overexpression in chick (Denans et al., 2015) and Hoxc13 overexpression in mouse caused a reduction in *wnt3a* levels (Young et al., 2009), demonstrating that our overexpression studies are causing similar changes to *brachyury* and Wnt signaling. Comparing our overexpression to loss of function effects side by side, we observed that overexpression of Hoxa13b also caused downregulation of the genes reduced in the *hoxa13;ntl*^{cs} mutant

embryos, as well as *fgf8a* and *cdx4*. However, Hoxa13b overexpression did not only cause an overall decrease in gene expression since other genes such as *bmp4*, *wnt5a* and *wnt16* increased under these conditions (Figure 7D and data not shown). From this data we conclude that overexpression of the *hox13* genes is not simply the opposite of loss of function, suggesting that the effects of Hox13 overexpression need to be interpreted cautiously.

DISCUSSION

Hoxa13b and Hoxd13a cooperate with Brachyury to establish the NMp niche

The Wnt/Brachyury autoregulatory loop is an essential feature of posterior development in early embryonic vertebrate development (Martin and Kimelman, 2008, 2009), with recent evidence from hemichordates demonstrating that it is an ancestral feature of deuterostomes (Fritzenwanker et al., 2019). In vertebrates, this loop ensures that cells remain in a bipotential progenitor state that can produce either neural or mesodermal fates. When canonical Wnt signaling is lost, embryos fail to produce mesoderm and neural tissue increases (Garriock et al., 2015; Gouti et al., 2017; Gouti et al., 2014; Jurberg et al., 2014; Martin and Kimelman, 2009; Nowotschin et al., 2012; Wymeersch et al., 2016). Thus, it is critical that the loop is maintained until the completion of posterior development. Brachyury has a second critical role of activating *cyp26a1* expression, thus keeping RA levels low at the posterior end of the vertebrate embryo since high RA inhibits mesoderm formation (Martin and Kimelman, 2010; Olivera-Martinez et al., 2012; Sive et al., 1990). We propose here that the *hox13* genes act to help create a niche at the posterior end of the embryo that has high Wnt and low RA by ensuring that the Wnt/Brachyury loop and Cyp26a1 are robustly expressed throughout much of the somite forming stages.

Key to our understanding of this pathway is the novel mutation in *tbxta* (*ntl*^{cs}), which allows us to control Tbxta activity depending on temperature (Kimelman, 2016a). Whereas *ntl*^{cs} mutants are indistinguishable from wildtype at the standard temperature of 28.5°C, when we reduce the temperature to 21°C we begin to see some posterior truncation phenotype, which is further enhanced at 18.5°C. But even at 18.5°C less than 10% of the embryos show the *ntl* null phenotype. This sensitized background was very useful for exploring the *hox13* mutants since the percentage of embryos with perturbed phenotypes

increased in embryos homozygous for a loss of *hoxa13b*, and even more so when *hoxd13a* was also mutant. Possibly the number of embryos with severe posterior truncations will increase yet further when the other less highly expressed posterior *hox13* genes (*hoxa13a*, *hoxc13a* and *hoxc13b*) are also mutant.

While the *hox13* genes have been proposed to act to terminate axis extension, we find that they are expressed very early in somitogenesis, with *hoxa13b* expressed at the start of somitogenesis, and *hoxd13a* expressed at the 8-somite stage, which seems surprising for their proposed role in terminating the axis. Similarly, a quantitative analysis in mouse has shown that *Hox13* genes are activated at E9.5 in the neuromesodermal progenitor region, whereas somitogenesis does not end until four days later (Wymeersch et al., 2019). In chick embryos, strong expression of the *Hox13* genes, as shown by in situ hybridization, was reported to begin around halfway through somitogenesis (Denans et al., 2015). While the timing of onset does not at all preclude the possibility that the *Hox13* genes are involved in axis termination, their early expression at least raises the possibility of alternate roles.

The evidence for *hox13* genes as axis terminators is based almost entirely on overexpression studies, with the one exception being the mouse *Hoxb13* mutant, which adds two somites to the tip of the tail increasing the body from 65 somites to 67, through enhanced proliferation and decreased cell death in the mesoderm and neural ectoderm (Economides et al., 2003), whereas all other *hox13* mutants show no effect on axis length (Dolle et al., 1993; Fromental-Ramain et al., 1996; Godwin and Capecchi, 1998; Suemori and Noguchi, 2000). Interestingly, the one zebrafish *hoxb13* gene, *hoxb13a*, is not expressed in the tailbud, and so perhaps the regulation of tailbud proliferation and apoptosis by *Hoxb13* is an amniote or mammalian adaptation.

While overexpression is commonly and often successfully used to study the role of different proteins in embryonic development, it can also lead to artifacts, particularly with transcription factors at higher than endogenous levels transcription factors could bind to aberrant binding sites in the genome. Moreover, since many transcription factors act in protein complexes, overexpression has the potential to disrupt the normal stoichiometry of the complex. In our overexpression studies using temporally controllable heat shock lines, we saw strong effects on embryonic posterior development when we overexpressed *hoxa13b*. Similarly, a previous study in zebrafish that mosaically overexpressed *hoxa13b*

using a promoter that restricted expression to the mesodermal progenitors and their descendants also observed defects on posterior development (Payumo et al., 2016), in agreement with our results. Why *hoxd13a* overexpression does not cause strong posterior defects is not yet clear, although it is in line with observations from overexpression studies in chick that also showed strong effects from *Hoxa13* overexpression but no effect from *Hoxd13* overexpression (Denans et al., 2015). While the DNA binding regions of the different Hox13 factors (the homeobox) are very highly conserved, the amino-terminus, which makes up almost all of the rest of the protein, is quite different between Hoxa13 and Hoxd13 proteins.

The most important finding from our overexpression studies is that in most cases the regulation of gene expression by overexpression is not the opposite of loss of function, raising concerns about interpreting overexpression studies of the Hox13 proteins. As was previously reported in mouse for *Hoxc13* overexpression (Young et al., 2009), we see a partial reduction in *wnt3a* expression when Hoxa13b is overexpressed, and a downregulation of *tbxta* expression under these conditions, in agreement with the reduction of *T/Brachyury* observed in chick embryos when *Hoxa13* is overexpressed (Denans et al., 2015). Thus, our overexpression results in general parallel those reported in amniotes. However, we also see a reduction in *tbxta* and *wnt3a* in the *hoxa13;ntl*^{cs} mutant embryos at the semi-permissive temperature of 18.5°C and also in the *hoxa13b;d13a;ntl*^{cs} mutants at 21°C (data not shown), demonstrating that the *hox13* genes promote the expression of these genes (and others), rather than inhibiting them. We therefore suggest that the previous overexpression studies should be carefully interpreted.

A new model for the role of the Hox13 genes

We propose that one key role of the *Hox13* genes is to provide robustness to the Wnt/Brachyury loop since it is critical that this loop is strongly expressed throughout all of the somitogenesis stages to ensure that mesoderm can be produced from the NMps as the body extends (Figure 8). If the loop fails at any point during somitogenesis due to decreased Wnt or Brachyury then the NMps fail to produce the somites and instead neural fates increase since only the *sox2*-positive derivatives of the NMps are produced (Garriock et al., 2015; Gouti et al., 2014; Martin and Kimelman, 2012; Tsakiridis et al., 2014; Turner et al., 2014). Wnt signaling is critical for the activation of downstream genes, particularly *tbx16* in

zebrafish and *Tbx6* and *Msgn1* in the mouse (Bouldin et al., 2015; Chalamalasetty et al., 2014; Kimelman, 2016b; Nowotschin et al., 2012; Wittler et al., 2007). These downstream genes act to inhibit the NMp state and to activate subsequent genes needed for somite formation (Figure 8). A second important role of Brachyury is to activate expression of the RA-degrading enzyme Cyp26a1 (Martin and Kimelman, 2010), which keeps the levels of RA low in the NMps since increased RA levels terminate axis extension. While RA is not necessary in mouse or zebrafish for terminating axis extension (Berenguer et al., 2018; Cunningham et al., 2011), it is essential that the levels in the posterior end of the embryo are kept very low (Martin and Kimelman, 2010; Olivera-Martinez et al., 2012; Sive et al., 1990).

The regulation of Wnt signaling in the tailbud is challenging for the embryo. In the NMps, Wnt signaling needs to be regulated at a level high enough for Brachyury expression to be maintained, but not so high as to force the cells into a mesodermal fate. Once the cells exit the most posterior end of the embryo and enter the posterior PSM, they are exposed to higher Wnt levels than is found in the NMp zone, which then activates mesodermal gene expression (Bouldin et al., 2015, Figure 8). However, if Wnt is too high throughout the tailbud it produces deleterious effect such as suppressed neural development (Jurberg et al., 2014 although see also Garriock et al., 2015; Martin and Kimelman, 2012), and aberrant segmentation (Bajard et al., 2014; Garriock et al., 2015; Jurberg et al., 2014). Thus, the role of the Hox13 genes might be to sustain the Wnt/Brachyury loop in the most posterior end of the embryo at a low level that is just sufficient to maintain Brachyury expression, but not so high as to cause deleterious effects.

How then might the Hox13 proteins regulate the Wnt/Brachyury loop? An intriguing possibility is suggested from a study in *C. elegans* that Hox factors act to ensure robust gene expression by consistently promoting the full activation of target genes by other transcription factors, and as such have been termed “guarantors” of gene expression (Zheng and Chalfie, 2016; Zheng et al., 2015). In the guarantor model, the Hox proteins are not absolutely required for target gene expression, and instead are critical in cases where due to variability in levels of transcription, some cells or groups of cells fall below a critical threshold of expression of an essential gene. In this sense, then, the variable and relatively low level of posterior embryonic defects seen at the fully permissive temperature (29°C) in

our cross of double mutant fish in the *ntl*$^{cs/cs}$ background can be viewed as embryos that stochastically fell on the lower end of expression of the Wnt/Brachyury loop due to very minor reductions in Tbxta activity without the help of the Hox13 factors to boost the levels. When Tbxta activity is further reduced in these embryos by lowering the temperature, the number of embryos that stochastically fall below the necessary threshold to sustain the loop increases, resulting in a greater number of embryos with a posterior defect. While a true test of this model will require eliminating all five tailbud-expressed *hox13* genes in zebrafish, it suggests that even a complete loss of Hox13 function may only be a partially penetrant effect with regards to completion of the anterior-posterior axis.

What genes are regulated by the Hox13 factors in any system remains unknown, but *tbxta/brachyury* is an intriguing candidate as it is upstream of both the *wnt* genes and *cyp26a1* (Martin and Kimelman, 2008, 2010), and its expression is strongly down-regulated in the *hoxa13;ntl*^{cs} embryos at the semi-permissive temperature (Figure 4). Interestingly, a DNA fragment containing just 2.1 kb upstream of the *tbxta* start site produced *tbxta* expression throughout the mesoderm during the gastrula stages, and later expression in the notochord, but it did not activate tailbud *tbxta* expression, demonstrating that proximal sequence of *tbxta* do not activate expression in the NMps during the somitogenesis stages (Harvey et al., 2010). Importantly, using a new method for identifying in vivo Hox13 binding sites in the tailbud cells has led to identification of a somitogenesis stage tailbud enhancer for *tbxta*, providing one clear locus of Hox13 regulation of the Wnt/Brachyury loop (Ye et al., in preparation).

METHODS

Mutants

Wildtype fish were an AB/WIK mixture. Fish were used for crosses between 3 months and 3 years old. The *ntl*^{cs} mutant fish (*ntla w181*) was previously described (Kimelman, 2016a).

In the *ntl*^{cs}*;hoxa13b*$^{\Delta 16}$ mutant (designated as line w243) 20 bp are deleted and 4 bp are added resulting in a 16 bp deletion. In the *hoxa13b* sequence CCCAAGTCCTGCACGCAACCCACCACATATGG is changed to CCCAAGagaaATATGG, with the lower case letters indicating novel bases.

In the *ntl*^{cs}*;hoxd13a*^{ins13} mutant (designated as line w244) 13 bp are inserted. In the *hoxd13a* sequence CCCGTGGACCAC is changed to CCCGTGaagcctcggtgaaGACCAC, with the lower case letters indicating novel bases.

In the *ntl*^{cs}*;hoxd13a*^{ins4} mutant (designated as line w245) 2 bp are deleted and 6 bp are added resulting in a 4 bp insertion. In the *hoxd13a* sequence AACCCGTGGACCAC is changed to AACCCGccaataGACCAC, with the lower case letters indicating novel bases.

In the *ntl*^{cs}*;hoxd13a*$^{\Delta 8}$ mutant (designated as line w246) 8 bp are deleted. In the *hoxd13a* sequence CAATAAACCCGTGGACCACGG is changed to CAATAAACCACGG.

All CRISPR mutant lines were designed and produced following published methods (Moreno-Mateos et al., 2015; Talbot and Amacher, 2014). The sequence used to make a gRNA for *hoxa13b* was GGGGGTTGCGTGCAGGACTT, which has a base change at the second base to allow for synthesis by T7 polymerase. The sequence used to make a gRNA for *hoxd13a* was GGGGCTTCACCGTGGTCCAC, which has a base change at the second base to allow for synthesis by T7 polymerase.

Transgenic lines

The *hoxa13b* and *hoxd13a* coding regions were amplified from 15s zebrafish embryo cDNA and inserted into a vector such that the stop codons were removed and a viral 2A peptide (Provost et al., 2007) was placed immediately after the coding region. The mCherry sequence was placed immediately after the 2A sequence. This sequence was placed in a Tol2-*hsp70* vector and the resulting plasmid was used together with Tol2 transposase to create stable transgenic lines as previously described (Kawakami, 2004): *hsp70l:hoxa13b-2A-mCherry* (designated w247) and *hsp70l:hoxd13a-2A-mCherry* (designated w248). Transgenic lines were heat shocked at 40°C for 30 mins.

All animal protocols used here were approved by the University of Washington Institutional Animal Care and Use Committee.

In situ hybridization

Alkaline phosphate in situ hybridization used standard conditions (https://wiki.zfin.org/display/prot/Thisse+Lab+-+In+Situ+Hybridization+Protocol+-+2010+update). Fluorescent in situ hybridization used a published procedure (Lauter et al., 2011).

Morpholino oligonucleotide

The sequence and use of the *tbxta/ntl* morpholino was previously described (Martin and Kimelman, 2008). Injected at 5 ng it completely recapitulates the *ntl* mutant phenotype.

Cell transplantation

Embryos were injected at the 1-cell stage with 2% fluorescein or rhodamine dextran, and transplanted into the ventral side of a shield stage wildtype embryo using a CellTram (Eppendorf). The *hoxa13;ntl*^{cs} donor embryos were also raised after a small number of cells were taken for transplantation and only donors that produced a strong phenotype were scored.

qPCR on tailbud explants

HS:hoxa13b and *HS:hoxd13a* embryos were heat shocked at 10s stage and kept at 28.5°C until they reached the 15s stage (about 3 hours post heatshock). *hoxa13;ntl*^{cs} embryos were

placed at 18.5°C at shield stage and kept at this temperature until sampling. Embryos were sorted either by mCherry expression for the transgenic embryos or by phenotype (large neural tube and small PSM) for the mutants. Wildtype control embryos were manipulated the same way as for each treatment. Tailbuds were isolated at the 15s stage using the method we described previously (Manning and Kimelman, 2015) in which the epidermis is removed prior to cutting the explant. The explants began at the boundary of the third most newly formed somite and extended to the most posterior end of the embryo. Thirty tailbuds were sampled and pooled for RNA extraction from each group. RNA was extracted using TriReagent (Invitrogen) and purified with RNA Clean & Concentrator spin columns (Zymo Research). cDNA was produced using the iScript Supermix cDNA kit (BioRad). QPCR was performed in triplicates using the SsoAdvanced Universal SYBR Green Supermix kit (BioRad) on a CFX Connect Real-Time PCR Detection System (BioRad). The primers used for amplification are listed in Table S1. The level of each specific gene in the explant was normalized to the level of *ribosomal 18S* mRNA in the explant, and the fold change of gene expression due to treatment (overexpression or mutation of *hoxa13b*) was calculated according to published methods (Schmittgen and Livak, 2008).

Cell tracking

Embryos were injected with 50 ng mRNA encoding H2B-EGFP synthesized in vitro from the plasmid CS2-H2B-EGFP using the mMESSAGE MACHINE SP6 kit (Invitrogen). Wildtype, *hoxa13;ntl*^{cs} and *tbxta* morphant embryos were placed at 18.5°C at shield stage and kept at this temperature until filming at the 10s stage. Embryos were mounted in 1% low-melt agrose and imaged using a spinning disk confocal microscope [inverted Marianas spinning disk system (Intelligent Imaging Innovations, 3i) with an Evolve 10 MHz EMCCD camera (Photometrics) and a Zeiss microscope Plan-NEOFLUAR 25X/0.8 immersion objective]. Time-lapse image stacks with a stepsize of 2 microns were taken every 2 minutes for a period of 2 hours at 25°C. *hoxa13;ntl*^{cs} and *tbxta* morphant embryos were retrieved from the agrose after imaging and allowed to develop to 2 dpf at 18.5°C to confirm phenotype. Three embryos from each genotype were used for the cell movement analysis using Imaris (Oxford Instruments).

QUANTIFICATION AND STATISTICAL ANALYSIS

Mann-Whitney test was used for comparison of the qPCR results for *mCherry* expression in the explants of *HS:hoxa13b* and *HS:hoxd13a* embryos after heatshock. Fisher's Exact test was used to compare the number of defective embryos (class 1, 2 and 3 phenotypes pooled) after 0.2 ng *tbxta* morpholino injection between the wildtype and *hoxa13;d13* mutant fish in a *ntl+/+* background.

For the cell movement data analysis, only tracks with a duration longer than 30 minutes were included. The mean track speed and straightness were calculated using Imaris. Tracks were color-coded by mean track speed or straightness using Imaris to generate Figure 6A, B, D, E, G, H. From each embryo, 300 to 500 representative tracks were manually and randomly picked from the NMp and MPZ based on the physical position. Tracks from the same region (NMp or MPZ) of three embryos were pooled for each genotype to do statistical analysis of cell movement. Dunn's test was used for the post hoc multiple comparisons of cell moving speed and straightness after detection of significant difference

by Kruskal-Wallis test. All the statistic analysis was conducted using R 3.6.0. The significance level for all the statistic analysis in this paper was set at $p < 0.05$.

Acknowledgements

We thank Natalie Smith and Adrian Wang for critical comments on the manuscript, Eric Thomas and Andrew Curtwright for advice on CRISPR, and Natalie Smith for invaluable help throughout this project. D.K. was supported by a grant from the National Institutes of Health (RO1GM079203).

Declaration of Interests

The authors declare no competing interests.

REFERENCES

Aires, R., de Lemos, L., Novoa, A., Jurberg, A.D., Mascrez, B., Duboule, D., and Mallo, M. (2019). Tail Bud Progenitor Activity Relies on a Network Comprising Gdf11, Lin28, and Hox13 Genes. Dev Cell *48*, 383-395 e388.

Amin, S., Neijts, R., Simmini, S., van Rooijen, C., Tan, S.C., Kester, L., van Oudenaarden, A., Creyghton, M.P., and Deschamps, J. (2016). Cdx and T Brachyury Co-activate Growth Signaling in the Embryonic Axial Progenitor Niche. Cell Rep *17*, 3165-3177.

Bajard, L., Morelli, L.G., Ares, S., Pecreaux, J., Julicher, F., and Oates, A.C. (2014). Wnt-regulated dynamics of positional information in zebrafish somitogenesis. Development *141*, 1381-1391.

Berenguer, M., Lancman, J.J., Cunningham, T.J., Dong, P.D.S., and Duester, G. (2018). Mouse but not zebrafish requires retinoic acid for control of neuromesodermal progenitors and body axis extension. Dev Biol *441*, 127-131.

Bouldin, C.M., Manning, A.J., Peng, Y.-H., Farr, G.H.I., Hung, K.L., Dong, A., and Kimelman, D. (2015). Wnt signaling and tbx16 form a bistable switch to commit bipotential progenitors to mesoderm Development *142*, 2499-2507.

Chalamalasetty, R.B., Garriock, R.J., Dunty, W.C., Jr., Kennedy, M.W., Jailwala, P., Si, H., and Yamaguchi, T.P. (2014). Mesogenin 1 is a master regulator of paraxial presomitic mesoderm differentiation. Development *141*, 4285-4297.

Cunningham, T.J., Zhao, X., and Duester, G. (2011). Uncoupling of retinoic acid signaling from tailbud development before termination of body axis extension. Genesis *49*, 776-783.

Das, D., Julich, D., Schwendinger-Schreck, J., Guillon, E., Lawton, A.K., Dray, N., Emonet, T., O'Hern, C.S., Shattuck, M.D., and Holley, S.A. (2019). Organization of Embryonic Morphogenesis via Mechanical Information. Dev Cell *49*, 829-839 e825.

Denans, N., Iimura, T., and Pourquie, O. (2015). Hox genes control vertebrate body elongation by collinear Wnt repression. Elife *4*.

Dolle, P., Dierich, A., LeMeur, M., Schimmang, T., Schuhbaur, B., Chambon, P., and Duboule, D. (1993). Disruption of the Hoxd-13 gene induces localized heterochrony leading to mice with neotenic limbs. Cell *75*, 431-441.

Economides, K.D., Zeltser, L., and Capecchi, M.R. (2003). Hoxb13 mutations cause overgrowth of caudal spinal cord and tail vertebrae. Dev Biol *256*, 317-330.

Fior, R., Maxwell, A.A., Ma, T.P., Vezzaro, A., Moens, C.B., Amacher, S.L., Lewis, J., and Saude, L. (2012). The differentiation and movement of presomitic mesoderm progenitor cells are controlled by Mesogenin 1. Development *139*, 4656-4665.

Fritzenwanker, J.H., Uhlinger, K.R., Gerhart, J., Silva, E., and Lowe, C.J. (2019). Untangling posterior growth and segmentation by analyzing mechanisms of axis elongation in hemichordates. Proc Natl Acad Sci U S A *116*, 8403-8408.

Fromental-Ramain, C., Warot, X., Messadecq, N., LeMeur, M., Dolle, P., and Chambon, P. (1996). Hoxa-13 and Hoxd-13 play a crucial role in the patterning of the limb autopod. Development *122*, 2997-3011.

Garnett, A.T., Han, T.M., Gilchrist, M.J., Smith, J.C., Eisen, M.B., Wardle, F.C., and Amacher, S.L. (2009). Identification of direct T-box target genes in the developing zebrafish mesoderm. Development *136*, 749-760.

Garriock, R.J., Chalamalasetty, R.B., Kennedy, M.W., Canizales, L.C., Lewandoski, M., and Yamaguchi, T.P. (2015). Lineage tracing of neuromesodermal progenitors reveals novel Wnt-dependent roles in trunk progenitor cell maintenance and differentiation. Development *142*, 1628-1638.

Godwin, A.R., and Capecchi, M.R. (1998). Hoxc13 mutant mice lack external hair. Genes Dev *12*, 11-20.

Gouti, M., Delile, J., Stamataki, D., Wymeersch, F.J., Huang, Y., Kleinjung, J., Wilson, V., and Briscoe, J. (2017). A Gene Regulatory Network Balances Neural and Mesoderm Specification during Vertebrate Trunk Development. Dev Cell *41*, 243-261 e247.

Gouti, M., Metzis, V., and Briscoe, J. (2015). The route to spinal cord cell types: a tale of signals and switches. Trends Genet *31*, 282-289.

Gouti, M., Tsakiridis, A., Wymeersch, F.J., Huang, Y., Kleinjung, J., Wilson, V., and Briscoe, J. (2014). In vitro generation of neuromesodermal progenitors reveals distinct roles for wnt signalling in the specification of spinal cord and paraxial mesoderm identity. PLoS Biol *12*, e1001937.

Griffin, K.J., Amacher, S.L., Kimmel, C.B., and Kimelman, D. (1998). Molecular identification of spadetail: regulation of zebrafish trunk and tail mesoderm formation by T-box genes. Development *125*, 3379-3388.

Halpern, M.E., Ho, R.K., Walker, C., and Kimmel, C.B. (1993). Induction of muscle pioneers and floor plate is distinguished by the zebrafish no tail mutation. Cell *75*, 99-111.

Harvey, S.A., Tumpel, S., Dubrulle, J., Schier, A.F., and Smith, J.C. (2010). no tail integrates two modes of mesoderm induction. Development *137*, 1127-1135.

Henrique, D., Abranches, E., Verrier, L., and Storey, K.G. (2015). Neuromesodermal progenitors and the making of the spinal cord. Development *142*, 2864-2875.

Holley, S.A. (2007). The genetics and embryology of zebrafish metamerism. Dev Dyn *236*, 1422-1449.

Jurberg, A.D., Aires, R., Novoa, A., Rowland, J.E., and Mallo, M. (2014). Compartment-dependent activities of Wnt3a/beta-catenin signaling during vertebrate axial extension. Dev Biol *394*, 253-263.

Kawakami, K. (2004). Transgenesis and gene trap methods in zebrafish by using the Tol2 transposable element. Methods Cell Biol *77*, 201-222.

Kimelman, D. (2016a). A novel cold-sensitive mutant of ntla reveals temporal roles of brachyury in zebrafish. Dev Dyn *245*, 874-880.

Kimelman, D. (2016b). Tales of tails (and trunks): forming the posterior body in vertebrate embryos. Curr Topics in Dev Biol *116*, 517-536.

Kimelman, D., and Martin, B.L. (2012). Anterior-Posterior patterning in early development: Three stratagies. WIREs Dev Biol *1*, 253-266.

Kimelman, D., Smith, N.L., Lai, J.K.H., and Stainier, D.Y. (2017). Regulation of posterior pody and epidermal morphogenesis in zebrafish by localized Yap1 and Wwtr1. eLife *6:e31065*, 1-29.

Lauter, G., Soll, I., and Hauptmann, G. (2011). Multicolor fluorescent in situ hybridization to define abutting and overlapping gene expression in the embryonic zebrafish brain. Neural Dev *6*, 10.

Lawton, A.K., Nandi, A., Stulberg, M.J., Dray, N., Sneddon, M.W., Pontius, W., Emonet, T., and Holley, S.A. (2013). Regulated tissue fluidity steers zebrafish body elongation. Development *140*, 573-582.

Ma, Z., Zhu, P., Shi, H., Guo, L., Zhang, Q., Chen, Y., Chen, S., Zhang, Z., Peng, J., and Chen, J. (2019). PTC-bearing mRNA elicits a genetic compensation response via Upf3a and COMPASS components. Nature *568*, 259-263.

Mallo, M. (2018). Reassessing the Role of Hox Genes during Vertebrate Development and Evolution. Trends Genet *34*, 209-217.

Manning, A.J., and Kimelman, D. (2015). Tbx16 and Msgn1 are required to establish directional cell migration of zebrafish mesodermal progenitors. Dev Biol *406*, 172-185.

Martin, B.L. (2016). Factors that coordinate mesoderm specification from neuromesodermal progenitors with segmentation during vertebrate axial extension. Semin Cell Dev Biol *49*, 59-67.

Martin, B.L., and Kimelman, D. (2008). Regulation of canonical Wnt signaling by Brachyury is essential for posterior mesoderm formation. Dev Cell *15*, 121-133.

Martin, B.L., and Kimelman, D. (2009). Wnt signaling and the evolution of embryonic posterior development. Curr Biol *19*, R215-219.

Martin, B.L., and Kimelman, D. (2010). Brachyury establishes the embryonic mesodermal progenitor niche. Genes Dev *24*, 2778-2783.

Martin, B.L., and Kimelman, D. (2012). Canonical Wnt signaling dynamically controls multiple stem cell fate decisions during vertebrate body formation. Dev Cell *22*, 223-232.

Mongera, A., Rowghanian, P., Gustafson, H.J., Shelton, E., Kealhofer, D.A., Carn, E.K., Serwane, F., Lucio, A.A., Giammona, J., and Campas, O. (2018). A fluid-to-solid jamming transition underlies vertebrate body axis elongation. Nature *561*, 401-405.

Moreno-Mateos, M.A., Vejnar, C.E., Beaudoin, J.D., Fernandez, J.P., Mis, E.K., Khokha, M.K., and Giraldez, A.J. (2015). CRISPRscan: designing highly efficient sgRNAs for CRISPR-Cas9 targeting in vivo. Nat Methods *12*, 982-988.

Morley, R.H., Lachani, K., Keefe, D., Gilchrist, M.J., Flicek, P., Smith, J.C., and Wardle, F.C. (2009). A gene regulatory network directed by zebrafish No tail accounts for its roles in mesoderm formation. Proc Natl Acad Sci U S A *106*, 3829-3834.

Morrow, Z.T., Maxwell, A.M., Hoshijima, K., Talbot, J.C., Grunwald, D.J., and Amacher, S.L. (2017). tbx6l and tbx16 are redundantly required for posterior paraxial mesoderm formation during zebrafish embryogenesis. Dev Dyn *246*, 759-769.

Nowotschin, S., Ferrer-Vaquer, A., Concepcion, D., Papaioannou, V.E., and Hadjantonakis, A.K. (2012). Interaction of Wnt3a, Msgn1 and Tbx6 in neural versus paraxial mesoderm lineage commitment and paraxial mesoderm differentiation in the mouse embryo. Dev Biol *367*, 1-14.

Olivera-Martinez, I., Harada, H., Halley, P.A., and Storey, K.G. (2012). Loss of FGF-dependent mesoderm identity and rise of endogenous retinoid signalling determine cessation of body axis elongation. PLoS Biol *10*, e1001415.

Payumo, A.Y., McQuade, L.E., Walker, W.J., Yamazoe, S., and Chen, J.K. (2016). Tbx16 regulates hox gene activation in mesodermal progenitor cells. Nat Chem Biol *12*, 694-701.

Pourquie, O. (2018). Somite formation in the chicken embryo. Int J Dev Biol *62*, 57-62.

Provost, E., Rhee, J., and Leach, S.D. (2007). Viral 2A peptides allow expression of multiple proteins from a single ORF in transgenic zebrafish embryos. Genesis *45*, 625-629.

Row, R.H., and Kimelman, D. (2009). Bmp inhibition is necessary for post-gastrulation patterning and morphogenesis of the zebrafish tailbud. Dev Biol *329*, 55-63.

Schmittgen, T.D., and Livak, K.J. (2008). Analyzing real-time PCR data by the comparative C(T) method. Nat Protoc *3*, 1101-1108.

Schulte-Merker, S., van Eeden, F.J., Halpern, M.E., Kimmel, C.B., and Nusslein-Volhard, C. (1994). no tail (ntl) is the zebrafish homologue of the mouse T (Brachyury) gene. Development *120*, 1009-1015.

Sive, H.L., Draper, B.W., Harland, R.M., and Weintraub, H. (1990). Identification of a retinoic acid-sensitive period during primary axis formation in Xenopus laevis. Genes Dev *4*, 932-942.

Steventon, B., and Martinez Arias, A. (2017). Evo-engineering and the cellular and molecular origins of the vertebrate spinal cord. Dev Biol *432*, 3-13.

Suemori, H., and Noguchi, S. (2000). Hox C cluster genes are dispensable for overall body plan of mouse embryonic development. Dev Biol *220*, 333-342.

Talbot, J.C., and Amacher, S.L. (2014). A streamlined CRISPR pipeline to reliably generate zebrafish frameshifting alleles. Zebrafish *11*, 583-585.

Tsakiridis, A., Huang, Y., Blin, G., Skylaki, S., Wymeersch, F., Osorno, R., Economou, C., Karagianni, E., Zhao, S., Lowell, S.*, et al.* (2014). Distinct Wnt-driven primitive streak-like populations reflect in vivo lineage precursors. Development *141*, 1209-1221.

Turner, D.A., Hayward, P.C., Baillie-Johnson, P., Rue, P., Broome, R., Faunes, F., and Martinez Arias, A. (2014). Wnt/beta-catenin and FGF signalling direct the specification and maintenance of a neuromesodermal axial progenitor in ensembles of mouse embryonic stem cells. Development *141*, 4243-4253.

Wilson, V., Olivera-Martinez, I., and Storey, K.G. (2009). Stem cells, signals and vertebrate body axis extension. Development *136*, 1591-1604.

Wittler, L., Shin, E.H., Grote, P., Kispert, A., Beckers, A., Gossler, A., Werber, M., and Herrmann, B.G. (2007). Expression of Msgn1 in the presomitic mesoderm is controlled by synergism of WNT signalling and Tbx6. EMBO Rep *8*, 784-789.

Wymeersch, F.J., Huang, Y., Blin, G., Cambray, N., Wilkie, R., Wong, F.C., and Wilson, V. (2016). Position-dependent plasticity of distinct progenitor types in the primitive streak. Elife *5*, e10042.

Wymeersch, F.J., Skylaki, S., Huang, Y., Watson, J.A., Economou, C., Marek-Johnston, C., Tomlinson, S.R., and Wilson, V. (2019). Transcriptionally dynamic progenitor populations organised around a stable niche drive axial patterning. Development *146*.

Yabe, T., and Takada, S. (2012). Mesogenin causes embryonic mesoderm progenitors to differentiate during development of zebrafish tail somites. Dev Biol *370*, 213-222.

Yamamoto, A., Amacher, S.L., Kim, S.H., Geissert, D., Kimmel, C.B., and De Robertis, E.M. (1998). Zebrafish paraxial protocadherin is a downstream target of spadetail involved in morphogenesis of gastrula mesoderm. Development *125*, 3389-3397.

Yoo, K.W., Kim, C.H., Park, H.C., Kim, S.H., Kim, H.S., Hong, S.K., Han, S., Rhee, M., and Huh, T.L. (2003). Characterization and expression of a presomitic mesoderm-specific mespo gene in zebrafish. Dev Genes Evol *213*, 203-206.

Young, T., Rowland, J.E., van de Ven, C., Bialecka, M., Novoa, A., Carapuco, M., van Nes, J., de Graaff, W., Duluc, I., Freund, J.N., *et al.* (2009). Cdx and Hox genes differentially regulate posterior axial growth in mammalian embryos. Dev Cell *17*, 516-526.

Zheng, C., and Chalfie, M. (2016). Securing Neuronal Cell Fate in C. elegans. Curr Top Dev Biol *116*, 167-180.

Zheng, C., Jin, F.Q., and Chalfie, M. (2015). Hox Proteins Act as Transcriptional Guarantors to Ensure Terminal Differentiation. Cell Rep *13*, 1343-1352.

Figures

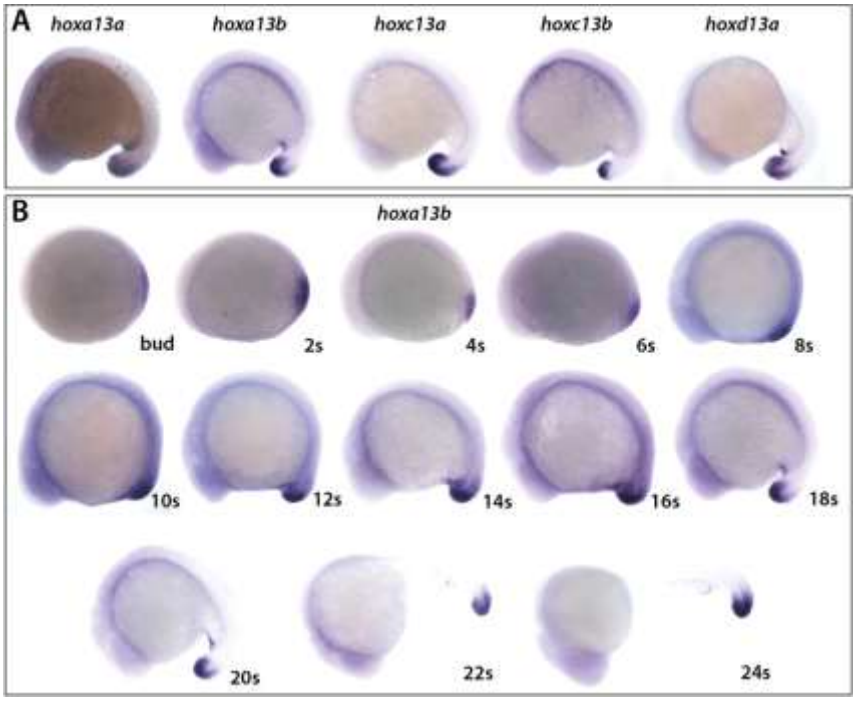

Figure 1 *hoxa13b* is expressed from early stages

A) Expression of the five posteriorly expressed *hox13* genes at 18 somites (s). The embryos were developed for different lengths of time to optimally show expression of each of the genes and do not reflect the relative levels of expression. B) Expression of *hoxa13b* from the end of gastrulation (bud stage) until 24s. Embryos from 8s to 24s were developed for the same length of time. Embryos from bud to 6s were developed 50% longer.

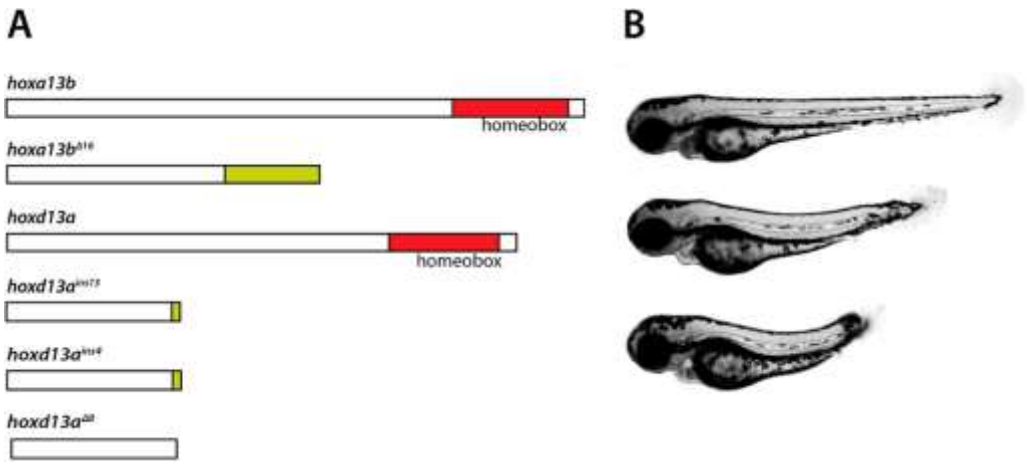

Figure *2 hoxa13;d13* mutants have posterior defects

A) Schematic diagram of *hox13* mutants. The coding regions of *hoxa13b* and *hoxd13a* are shown, with the DNA binding homeobox indicated. The *hoxa13b*$^{\Delta 16}$ mutant is truncated due to a 16 base pair (bp) deletion that causes a frameshift, adding additional amino acids (green). Three *hoxd13a* mutants are shown which cause an insertion of 13 or 4 bp or a deletion of 8 bp. The 8 bp deletion causes an immediate truncation whereas the insertion mutants cause frameshifts that add a small number of additional amino acids. B) Posterior defects observed in *hoxa13*$^{\Delta 16}$*;hoxd13a*^{ins13} mutants (lower two embryos) compared to a wildtype embryo (top) at 3 days post-fertilization.

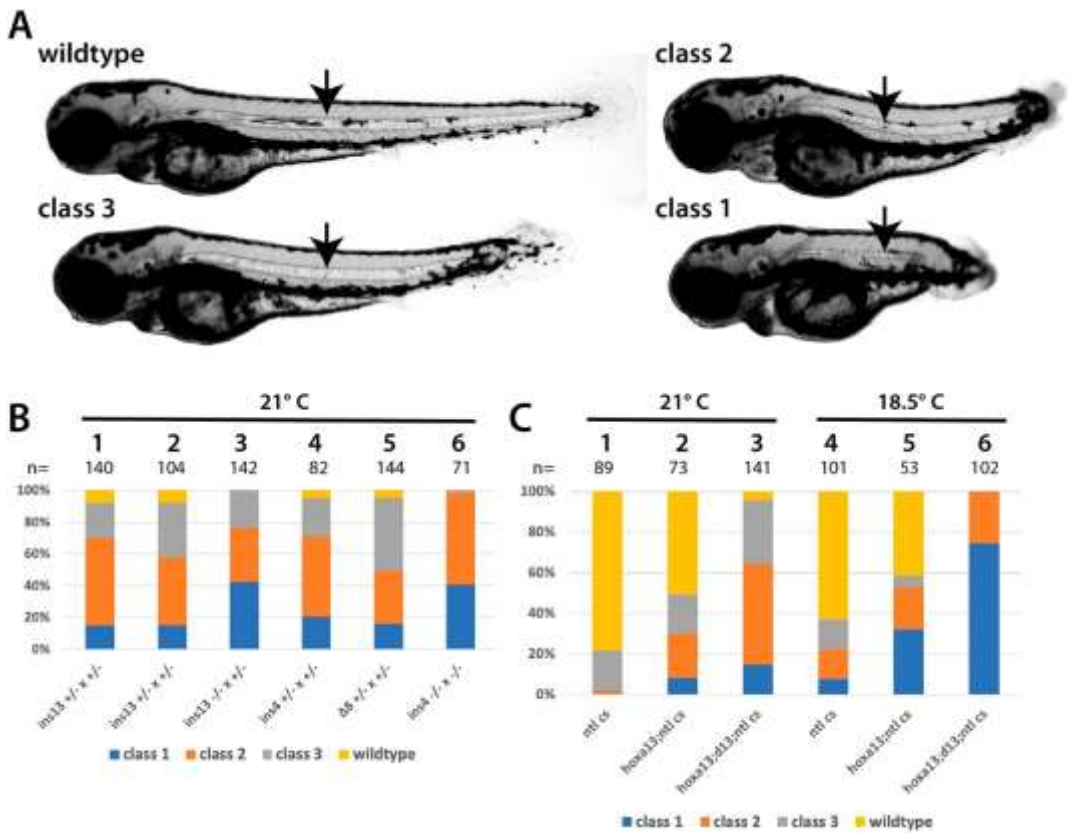

Figure 3 Interaction between the *hox13* genes and *tbxta/ntl*

A) Classification used to score embryos at 3 days post-fertilization (dpf). The strongest class, class 1, has the same phenotype as *tbxta/ntl* mutants. Class 2 mutants have a clearly truncated axis, and extend beyond the anus at the end of the yolk tube. Class 3 mutants have relatively minor posterior defects. All classes of embryos have a notochord (arrow). B) Embryos raised from different crosses that were placed at 21°C at shield stage and scored at 3 dpf. The specific *hoxd13a* mutation is shown; all fish were homozygous for both *hoxa13b*$^{\Delta 16}$ and *ntl*^{cs}. The embryos shown in columns 1 and 2 are from two separate families with the same genotype. C) Embryos raised from different crosses that were placed at 21°C or 18.5°C at shield stage and scored at 3 dpf. The labels in each column of the adults used in the cross are: *ntl cs*, homozygous for *ntl*^{cs}; *hoxa13;ntl cs*, homozygous for both *hoxa13b*$^{\Delta 16}$ and *ntl*^{cs}; *hoxa13;d13;ntl cs*, homozygous for both *hoxa13b*$^{\Delta 16}$ and *ntl*^{cs} and heterozygous for *hoxd13a*^{ins13}.

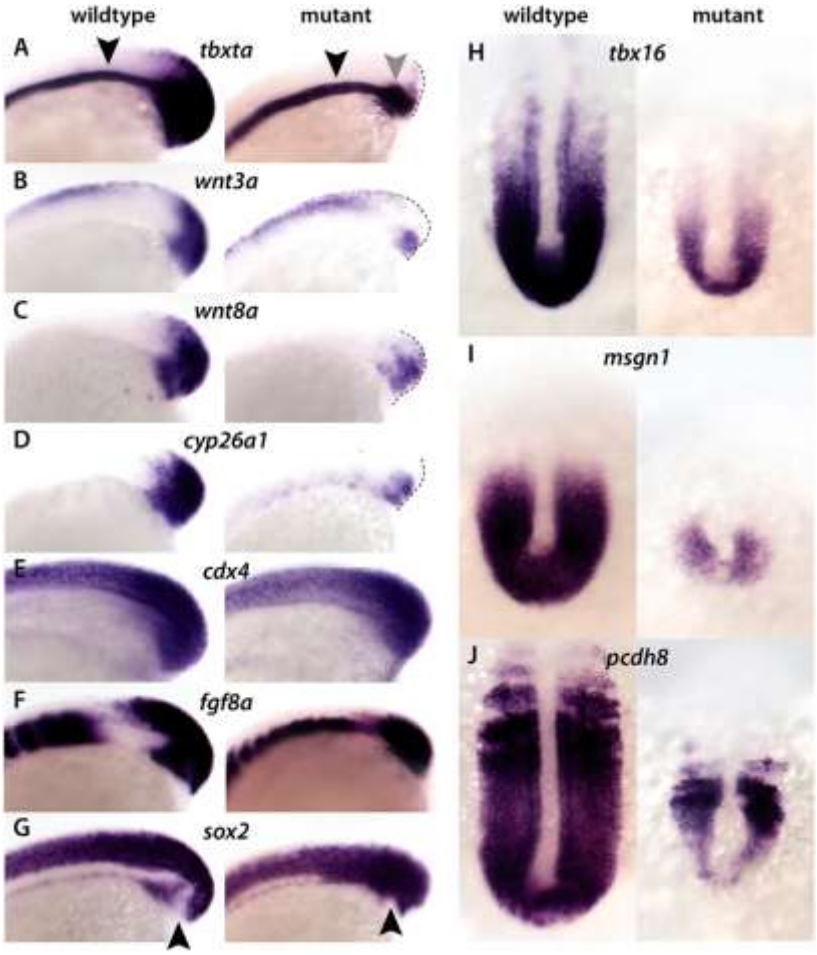

Figure 4 Mesodermal defects in *hoxa13;ntl*^{cs} embryos maintained at 18.5°C.

A-J) In situ hybridization of 15s wildtype and *hoxa13;ntl*^{cs} embryos. A) *tbxta*. In mutant embryos the expression at the posterior end (NMp domain) of the embryo is absent, whereas the expression in the notochord progenitors (gray arrowhead) is retained. Note that in mutant embryos *tbxta* expression in the notochord is normal (black arrowheads). B-D) Expression of *wnt3a* (B), *wnt8a* (C) and *cyp26a1* (D) are strongly downregulated in the posterior in mutant embryos. E, F) Expression of *cdx4* (E) and *fgf8a* (F) are largely normal or only partially reduced in the posterior of mutant embryos. G) *sox2* expression expands into the mesodermal progenitor region in the mutants whereas in wildtype embryos *sox2* is absent from this region (black arrowheads). H-J) *tbx16* (H), *msgn1* (I) and *pcdh8* (J) are strongly downregulated in mutant embryos. Panels A-G show side views and panels H-J show dorsal views.

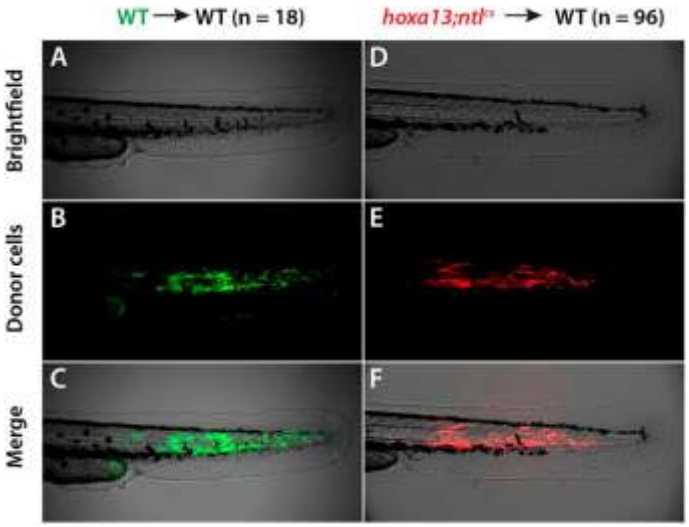

Figure 5 *hoxa13;ntl*^{cs} cells are rescued for differentiation in a wildtype environment

(A-F) Donor embryos were injected with a fluorescent dye, and then 30-50 cells from each donor were transplanted into the prospective tail mesoderm of a wildtype host embryo at shield stage. At 2 dpf the embryos were imaged. Wildtype donor cells contribute to tail muscle, producing elongated muscle cells within the somites (A-C). Cells from *hoxa13;ntl*^{cs} also contribute to tail muscle (D-F).

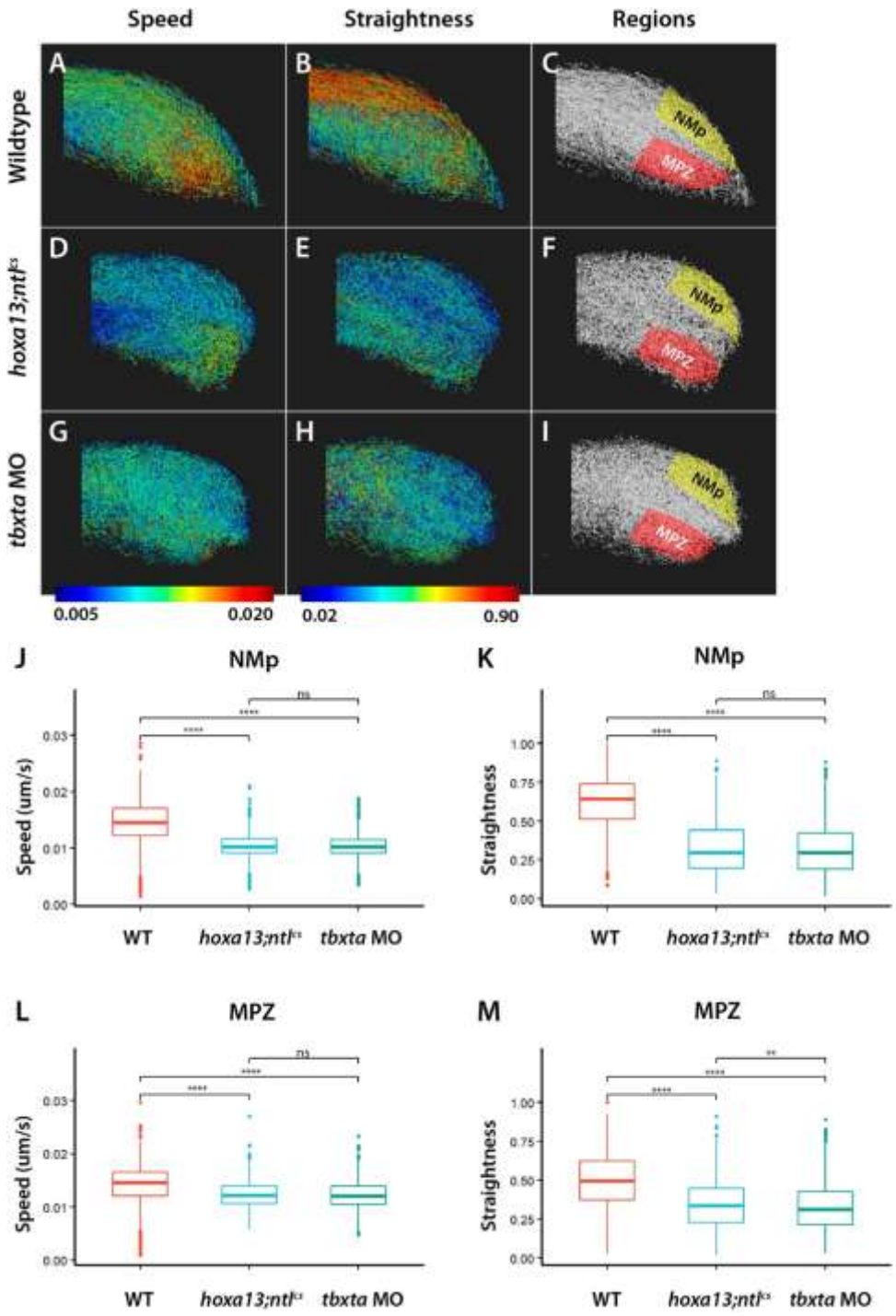

Figure 6 *hoxa13;ntl*^{cs} mutants and *tbxta* morphants have similar posterior cell movements

(A-I) Embryos expressing nuclear EGFP were filmed at the posterior end. Tracks from a representative embryo is shown in each panel, with the lowest speed or straightness shown in blue and the highest in red. The regions used for quantitative analysis are shown on the right side with the NMps and mesodermal progenitor zone (MPZ) illustrated. Note the similar shapes of the tailbuds of *hoxa13;ntl*^{cs} mutants and *tbxta* morphants (*tbxta* MO)

compared to wildtype. (J-M) Graphs of speed (J,L) and straightness (K,M) obtained from analysis of 1193, 1295, 1396 tracks from the NMps and 1173, 1273, 1399 tracks from the MPZ of three wildtype, *hoxa13;ntlcs* mutant and *tbxta* morphant embryos, respectively. The speed is shown in um/sec. Straightness is the displacement divided by the track length, a value of 1.0 indicates movement in a perfectly straight direction whereas a value of 0.0 indicates no displacement from the origin. Dunn's test was used for multiple comparisons of mean speed and straightness. **: $p < 0.01$; ****: $p < 0.001$; ns: no significant difference ($p > 0.05$).

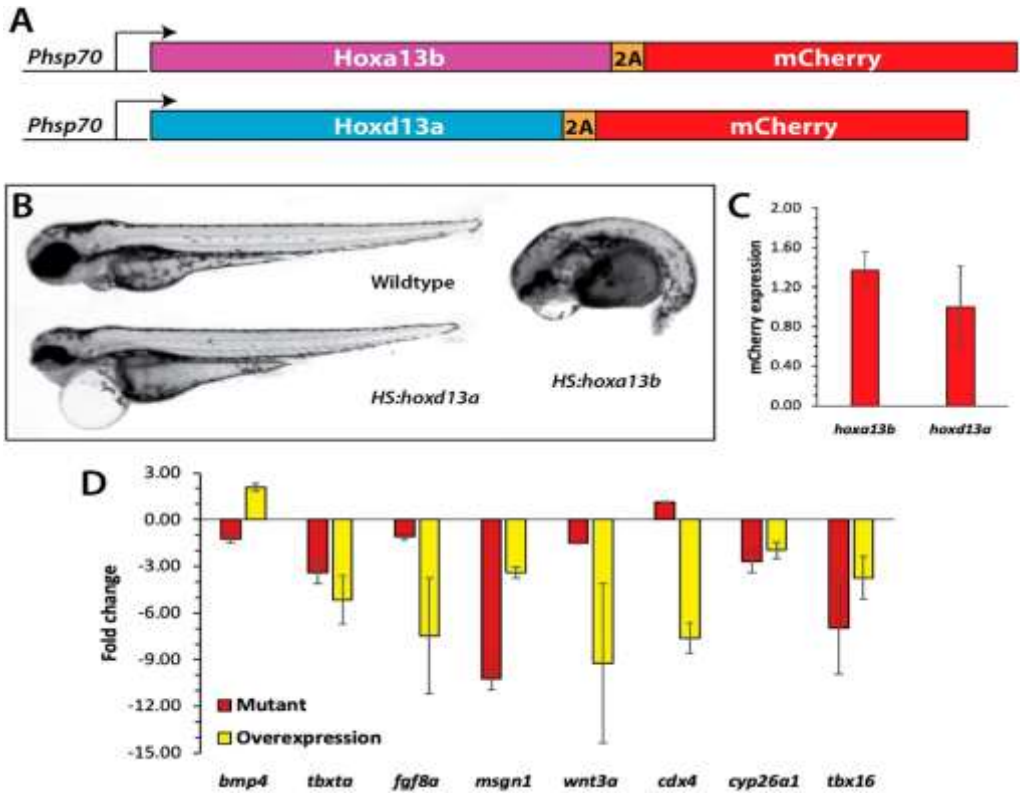

Figure 7 Analysis of Hox13 overexpression

A) Constructs used to overexpress Hoxa13b and Hoxd13a. The coding region of each gene was placed under the control of a *hsp70l* promoter, and placed in frame with the 2A peptide and mCherry, which allows both the Hox13 protein and mCherry to be produced as one transcript and two separate proteins. B) Wildtype and transgenic embryos were heat shocked at 10s and then analyzed at 2 dpf. Embryos overexpressing Hoxa13b had posterior truncations, whereas embryos overexpressing Hoxd13a had normal posteriors with minor anterior defects, often including pericardial edema. We observed the same phenotype from Hoxa13b overexpression in $ntl^{+/+}$, $ntl^{cs/+}$ and $ntl^{cs/cs}$ backgrounds (data not shown). C) The levels of *mCherry* expression (mean $\pm$ SD) was measured by qPCR in tailbud explants isolated from embryos heat shocked as in panel B. The differences in *mCherry* expression was not significant (Mann-Whitney test, $p = 0.4$). D) Fold changes of gene expression in *hoxa13;*ntl^{cs} mutant embryos and embryos overexpressing Hoxa13b. Data from three independent replicates. Only *bmp4* showed opposite effects in the two conditions. *cdx4* in the mutant embryos was unchanged compared to wildtype. Note that the tailbud explants include the posterior notochord and neural tube, and thus, the decrease in *tbxta* and *wnt3a* expression in the mutants is not as strong as shown by in situ hybridization (Figure 4) due to their expression in these other tissues.

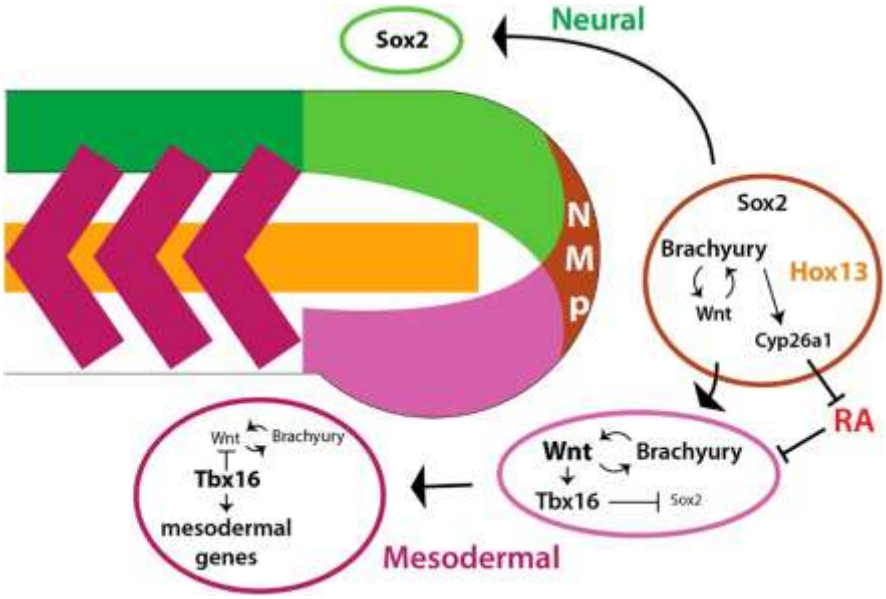

Figure 8 Model for formation of the neural and mesodermal tissues from the NMps.

A model based on work presented here and from other studies. The NMps co-express Sox2 and Brachyury/Tbxta. Cells that migrate into a Wnt-free environment retain Sox2 expression and differentiate as neural cells. Cells that enter a high Wnt environment retain Brachyury expression and activate Tbx16 (Tbx6 in amniotes), which together with Msgn1 and Tbx16l (Morrow et al., 2017), activates mesodermal gene expression. Tbx16 also represses both Sox2 and later Wnt, to promote mesodermal differentiation (Bouldin et al., 2015). Brachyury has an essential role in creating the niche for mesoderm formation by activating canonical Wnt expression and inhibiting RA from the posterior end by inducing the expression of Cyp26a1. We propose that the Hox13 proteins act within the NMps to enhance the niche-promoting effects of Brachyury.

SUPPLEMENTARY FIGURES

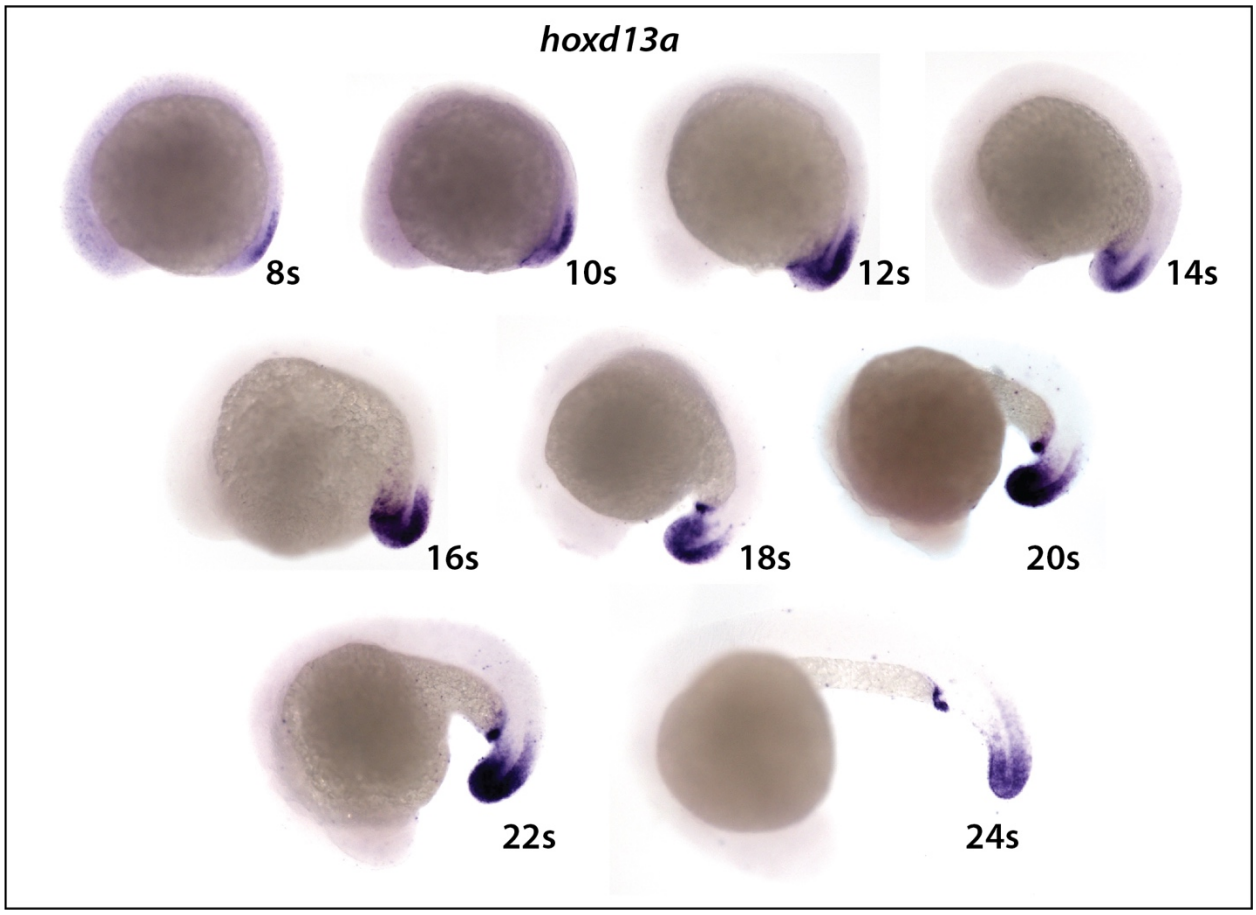

Figure S1 *hoxd13a* is expressed from early stages of embryogenesis. Refers to Figure 1.

Expression of *hoxd13a* from 8s until the 24s. Embryos from 12s to 24s were developed for the same length of time. Embryos at 8s and 10s were developed twice as long.

Figure S2 Adult *hoxa13b;d13a* mutant. Refers to Figure 2.

Shown is a *ntl*$^{cs/cs}$;*hoxa13b*$^{\Delta 16/\Delta 16}$;*d13b*$^{ins4/-}$ mutant that survived to adulthood with severe posterior defects. Most fish with this degree of posterior defect die as larvae.

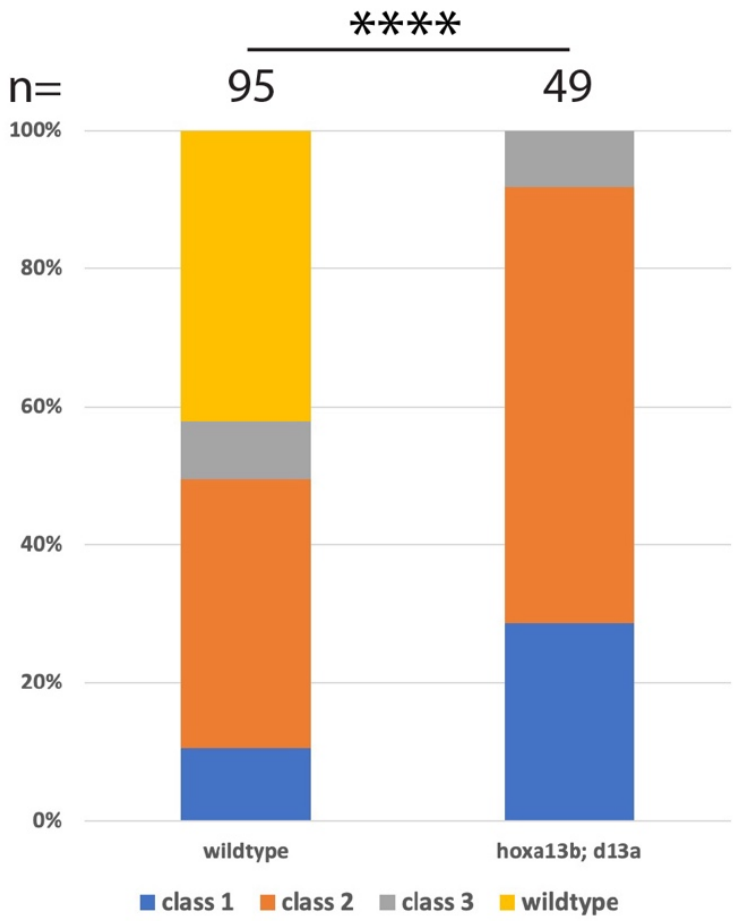

Figure S3 *Hoxa13b;d13a* mutants in a *ntl* wildtype background are hypersensitive to Tbxta reduction. Refers to Figure 3.

Embryos from a cross of wildtype or *hoxa13;d13* mutant fish (in a $ntl^{+/+}$ background) were injected with very low doses (0.2 ng) of a *tbxta* morpholino. The *hoxa13;d13* mutant fish show enhanced defects relative to wildtype fish. **** = p<0.0001, Fisher's Exact test.

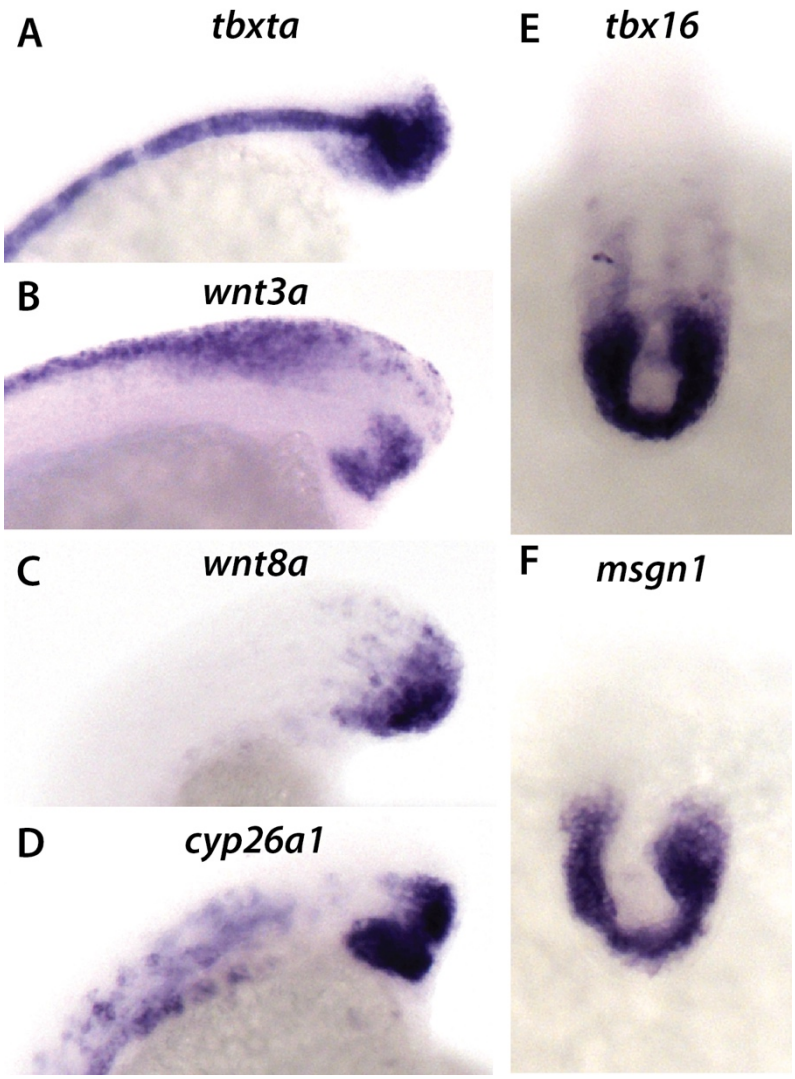

Figure S4 Reduction of mesodermal gene expression in *ntl*^{cs} embryos at 18.5° C. Refers to Figure 4.

A-F) In situ hybridization of class 1 15s *ntl*^{cs} homozygous embryos maintained at 18.5° C. Compare to the wildtype expression patterns shown in Figure 4. The reduction of mesodermal genes is the same as observed in in *hoxa13;ntl*^{cs} embryos maintained at 18.5°C.

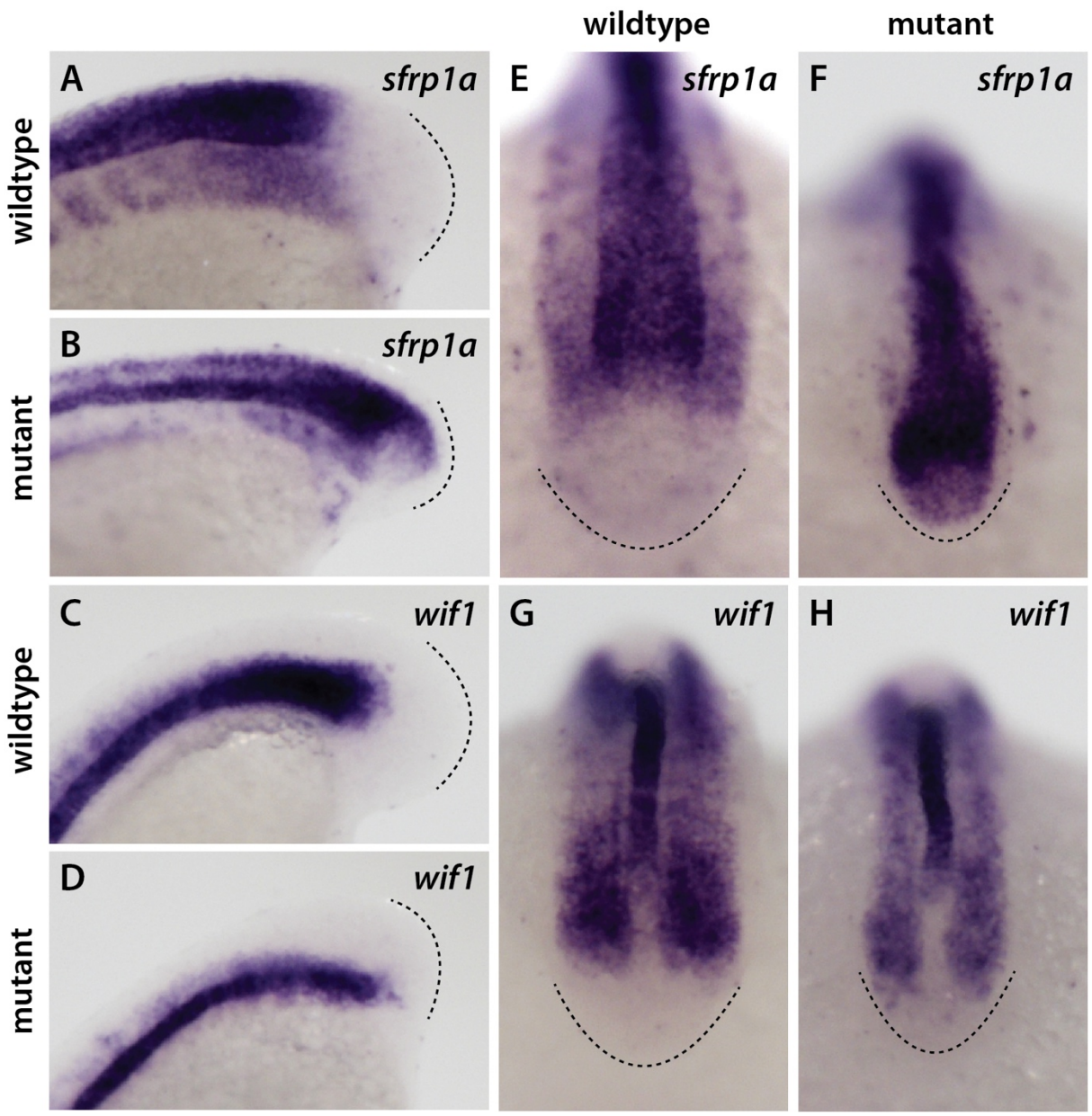

Figure S5 Wnt inhibitors expressed more posteriorly in *hoxa13;ntl*^{cs} embryos at 18.5° C. Refers to Figure 4.

(A-H) In situ hybridization of wildtype and *hoxa13;ntl*^{cs} embryos at 15s. Note that both genes expand more posteriorly in the mutants. Mutants with expanded expression: *sfrp1a* (81%, n=26) and *wif1* (79%, n=24). A-D are lateral views and panels E-H are dorsal views. The posterior limit of the tailbud is shown by a line.

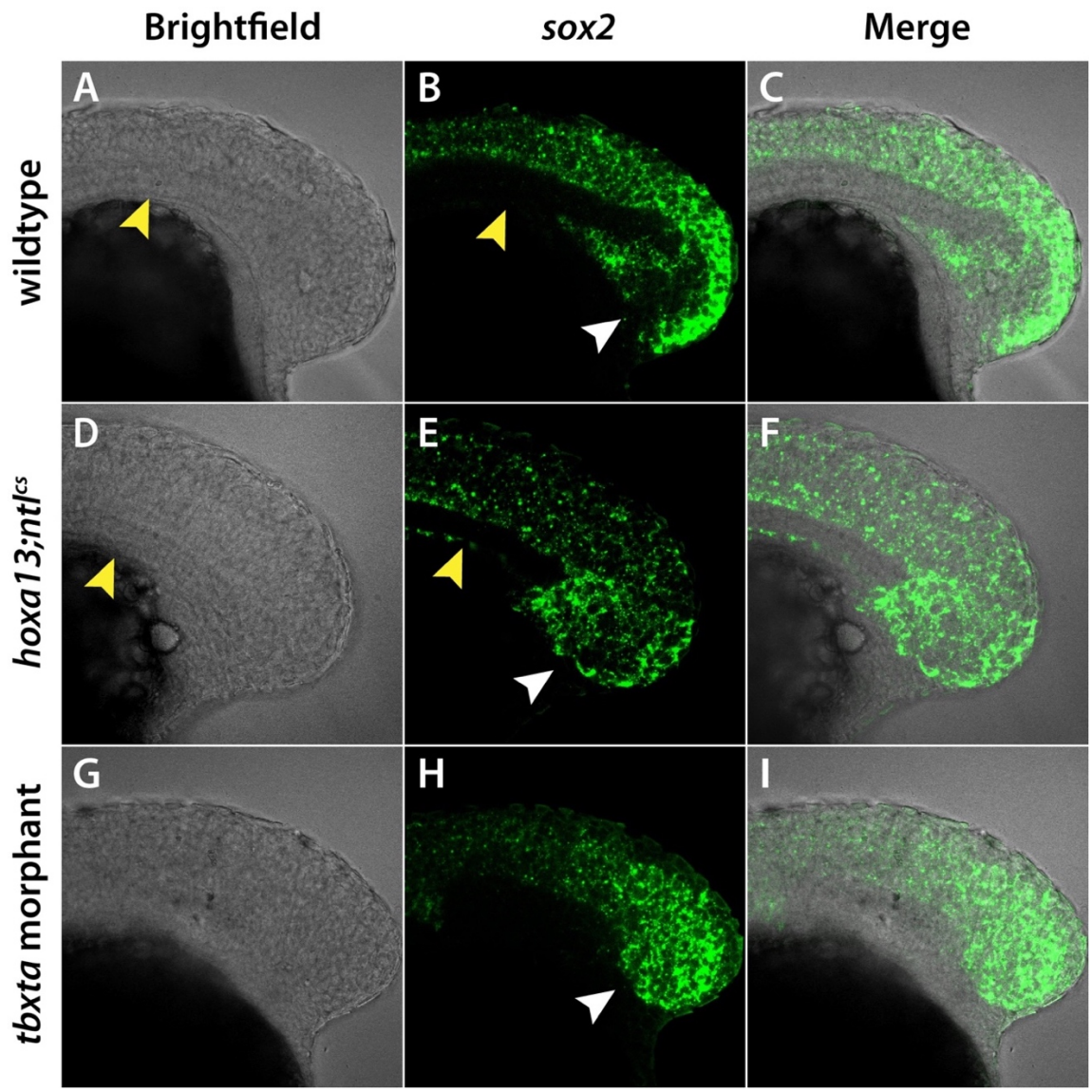

Figure S6 *sox2* expression expands into the mesodermal progenitor region in *hoxa13;ntl*^{cs} mutants at 18.5° C.

A-C) In wildtype embryos *sox2* is present in the NMps and neural tube, but absent from the mesodermal progenitor zone (white arrowhead). D-F) In *hoxa13;ntl*^{cs} mutants *sox2* expands into the mesodermal progenitor zone (white arrowhead). F-I) in *tbxta/ntl* morphants *sox2* also expands into the mesodermal progenitor zone, as was previously shown for *tbxta/ntl* mutants (Martin and Kimelman, 2012). In both brightfield and fluorescent imaging the notochord is visible in wildtype and *hoxa13;ntl*^{cs} mutants (yellow arrowheads in panels A,B,D and E) but is not observed in *tbxta/ntl* morphants. Embryos are at the 15s stage and are shown in a side view of a confocal section at the midline of the embryo.

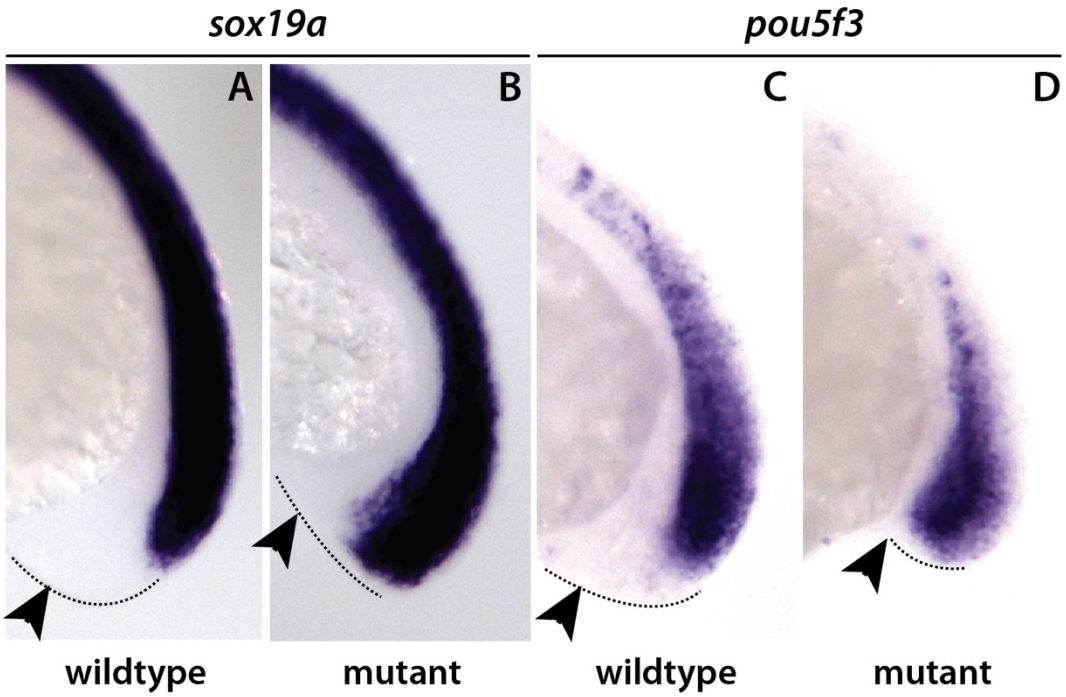

Figure S7 *sox19a and pou5f3* expression expands into the mesodermal progenitor region in *hoxa13;ntl^{cs}* mutants at 18.5° C. Refers to Figure 4.

A-D) In situ hybridization of 15s wildtype and *hoxa13;ntl^{cs}* embryos for the neural markers *sox19a* and *pou5f3*. As with *sox2*, expression expands into the prospective mesodermal territory in the *hoxa13;ntl^{cs}* mutants.

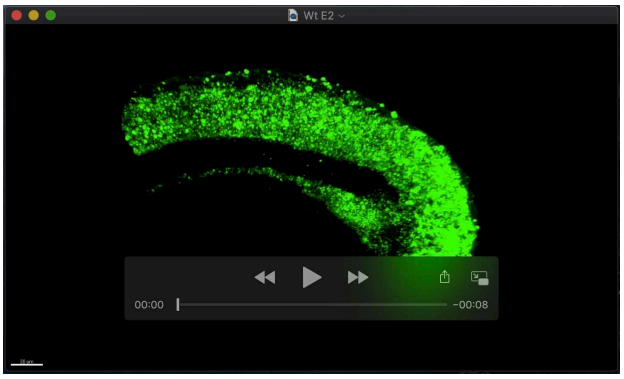

Movie 1

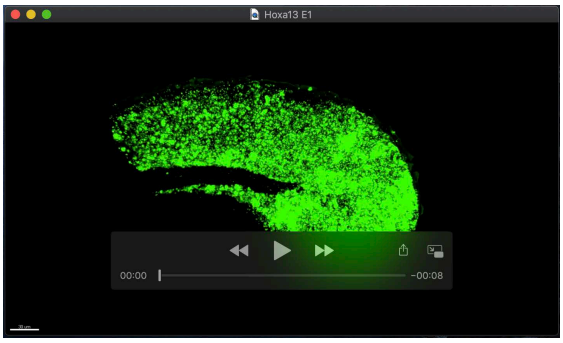

Movie 2

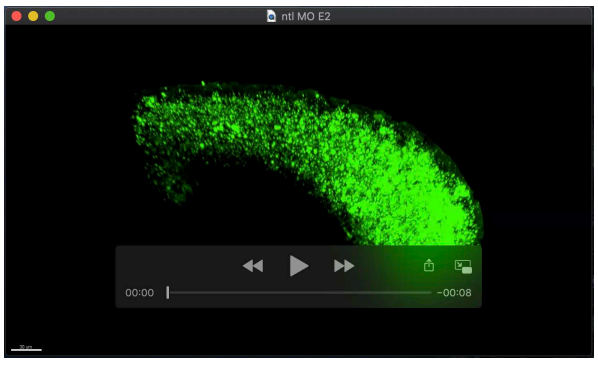

Movie 3

SUPPLEMENTARY FIGURES

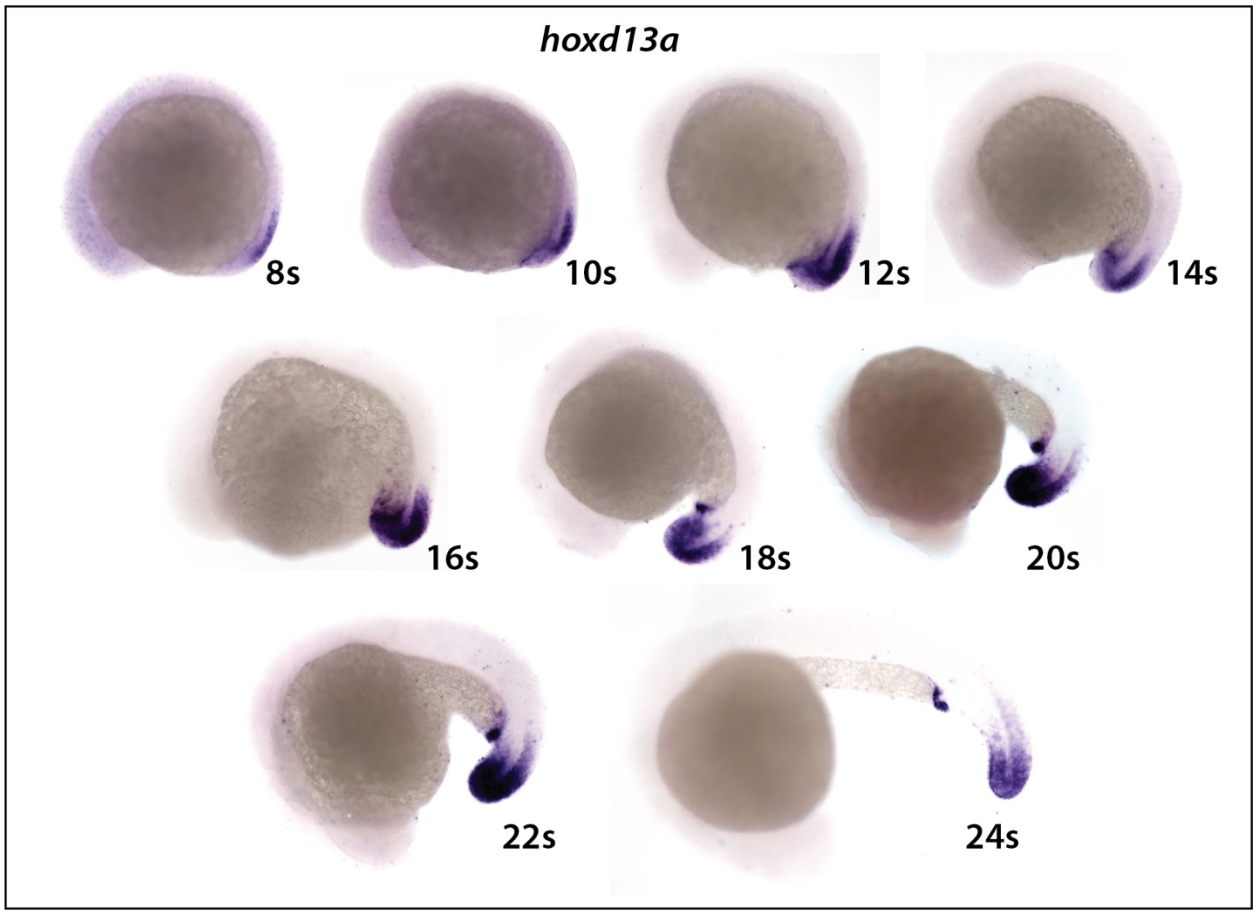

Figure S1 *hoxd13a* is expressed from early stages of embryogenesis. Refers to Figure 1.

Expression of *hoxd13a* from 8s until the 24s. Embryos from 12s to 24s were developed for the same length of time. Embryos at 8s and 10s were developed twice as long.

Figure S2 Adult *hoxa13b;d13a* mutant. Refers to Figure 2.

Shown is a *ntl*$^{cs/cs}$;*hoxa13b*$^{\Delta 16/\Delta 16}$;*d13b*$^{ins4/-}$ mutant that survived to adulthood with severe posterior defects. Most fish with this degree of posterior defect die as larvae.

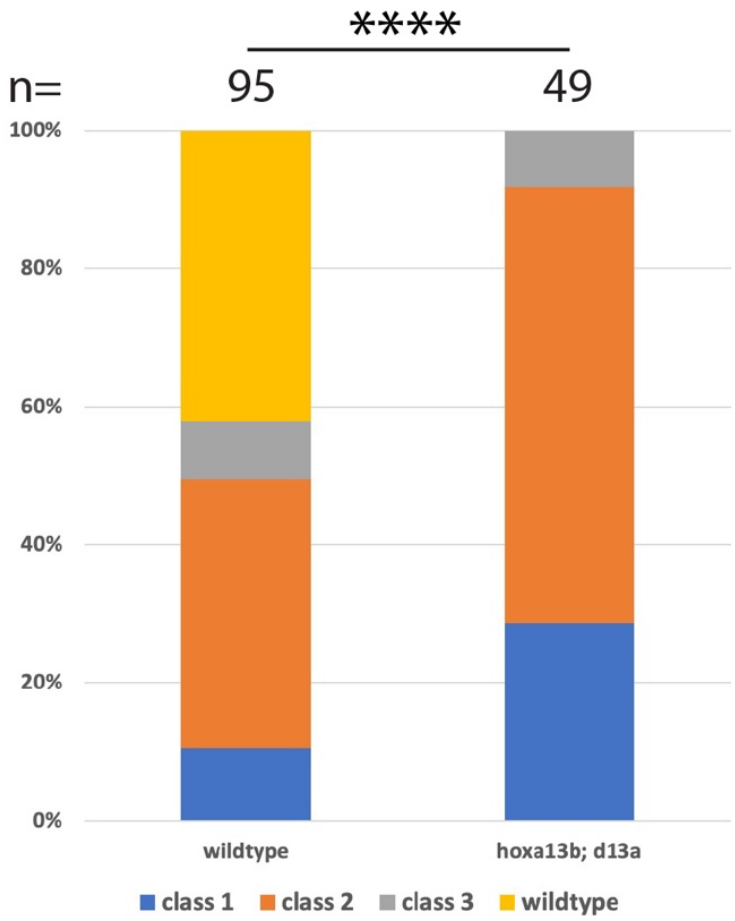

Figure S3 *Hoxa13b;d13a* mutants in a *ntl* wildtype background are hypersensitive to Tbxta reduction. Refers to Figure 3.

Embryos from a cross of wildtype or *hoxa13;d13* mutant fish (in a $ntl^{+/+}$ background) were injected with very low doses (0.2 ng) of a *tbxta* morpholino. The *hoxa13;d13* mutant fish show enhanced defects relative to wildtype fish. **** = p<0.0001, Fisher's Exact test.

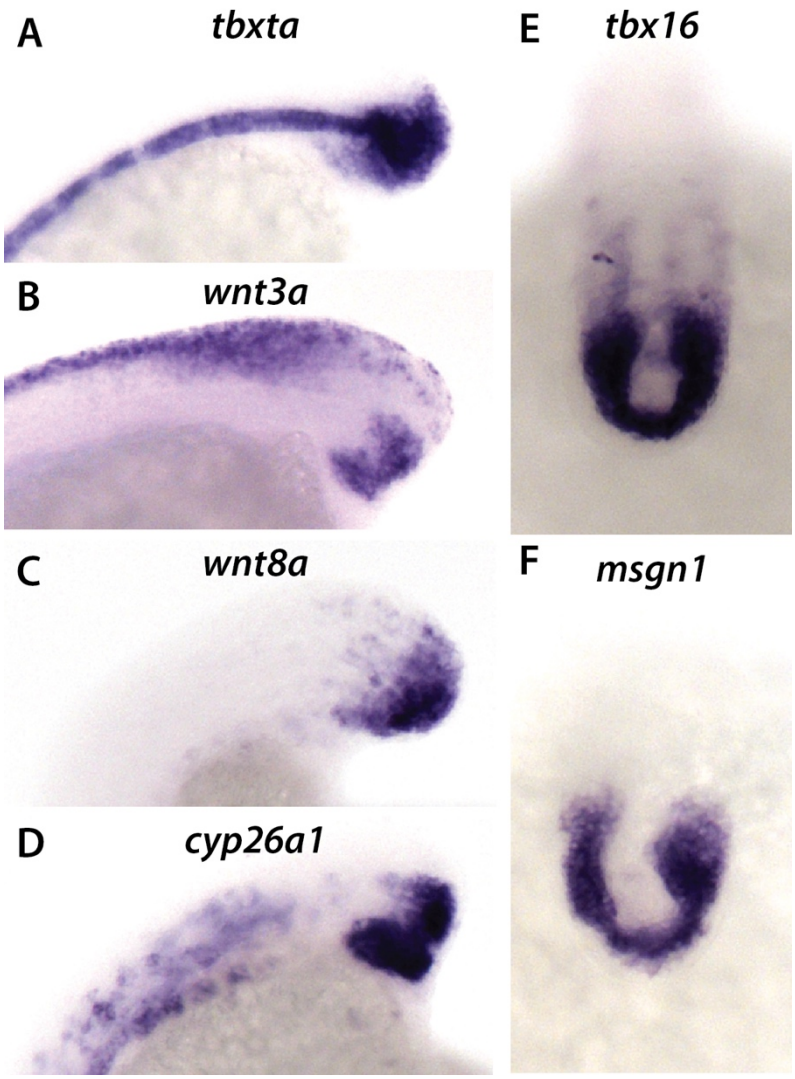

Figure S4 Reduction of mesodermal gene expression in *ntl*^{cs} embryos at 18.5° C. Refers to Figure 4.

A-F) In situ hybridization of class 1 15s *ntl*^{cs} homozygous embryos maintained at 18.5° C. Compare to the wildtype expression patterns shown in Figure 4. The reduction of mesodermal genes is the same as observed in in *hoxa13;ntl*^{cs} embryos maintained at 18.5°C.

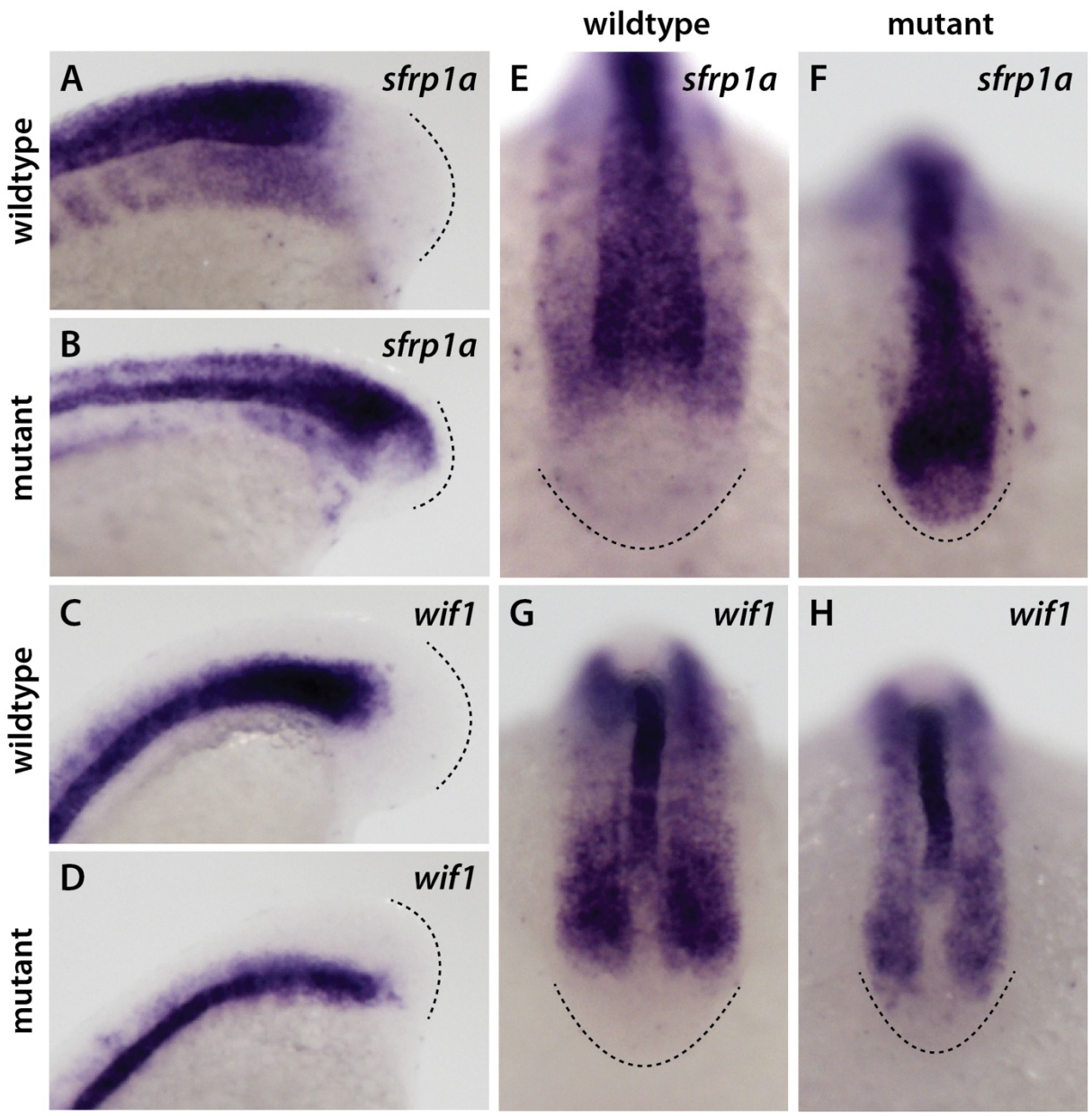

Figure S5 Wnt inhibitors expressed more posteriorly in *hoxa13;ntl*^{cs} embryos at 18.5° C. Refers to Figure 4.

(A-H) In situ hybridization of wildtype and *hoxa13;ntl*^{cs} embryos at 15s. Note that both genes expand more posteriorly in the mutants. Mutants with expanded expression: *sfrp1a* (81%, n=26) and *wif1* (79%, n=24). A-D are lateral views and panels E-H are dorsal views. The posterior limit of the tailbud is shown by a line.

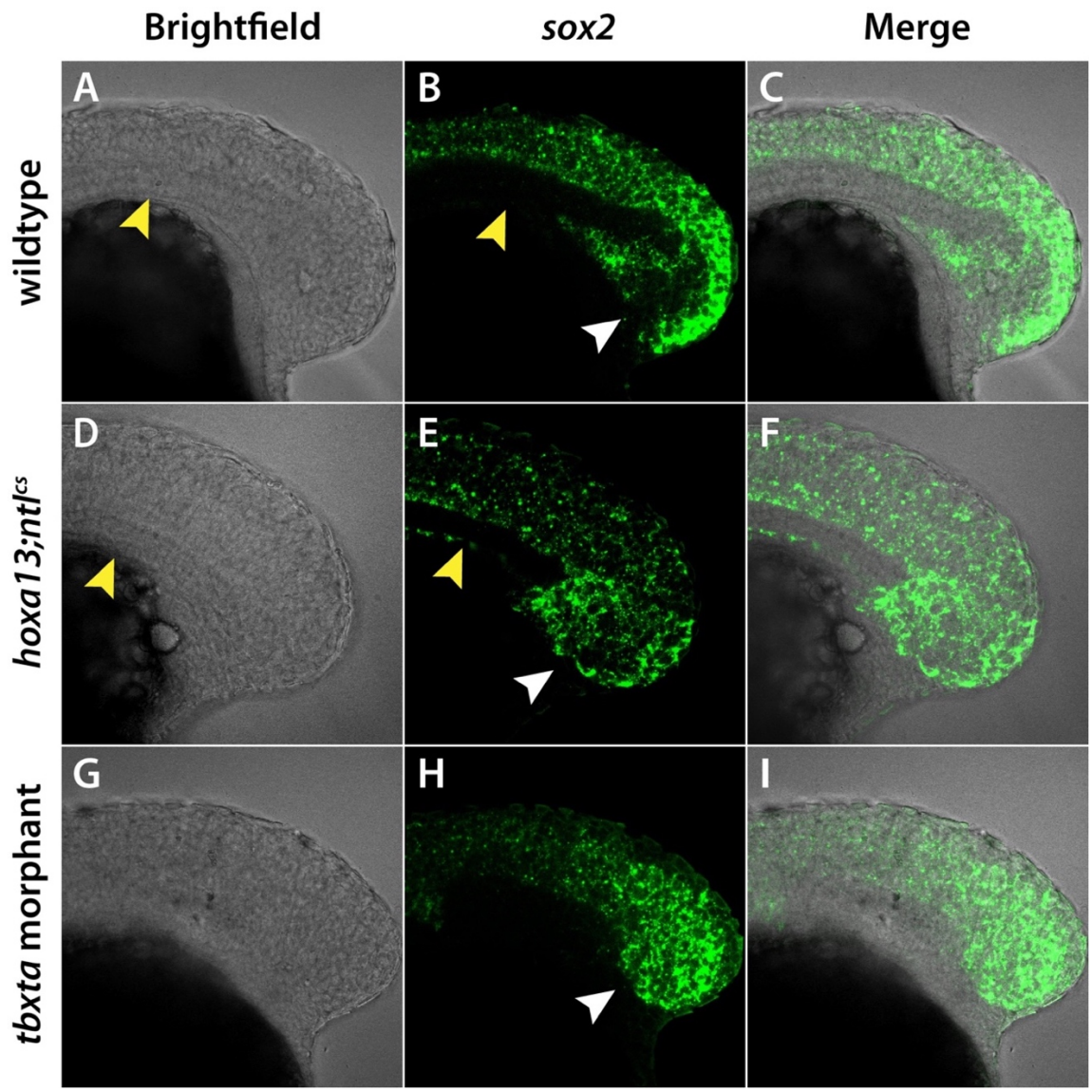

Figure S6 *sox2* expression expands into the mesodermal progenitor region in *hoxa13;ntl*^{cs} mutants at 18.5° C.

A-C) In wildtype embryos *sox2* is present in the NMps and neural tube, but absent from the mesodermal progenitor zone (white arrowhead). D-F) In *hoxa13;ntl*^{cs} mutants *sox2* expands into the mesodermal progenitor zone (white arrowhead). F-I) in *tbxta/ntl* morphants *sox2* also expands into the mesodermal progenitor zone, as was previously shown for *tbxta/ntl* mutants (Martin and Kimelman, 2012). In both brightfield and fluorescent imaging the notochord is visible in wildtype and *hoxa13;ntl*^{cs} mutants (yellow arrowheads in panels A,B,D and E) but is not observed in *tbxta/ntl* morphants. Embryos are at the 15s stage and are shown in a side view of a confocal section at the midline of the embryo.

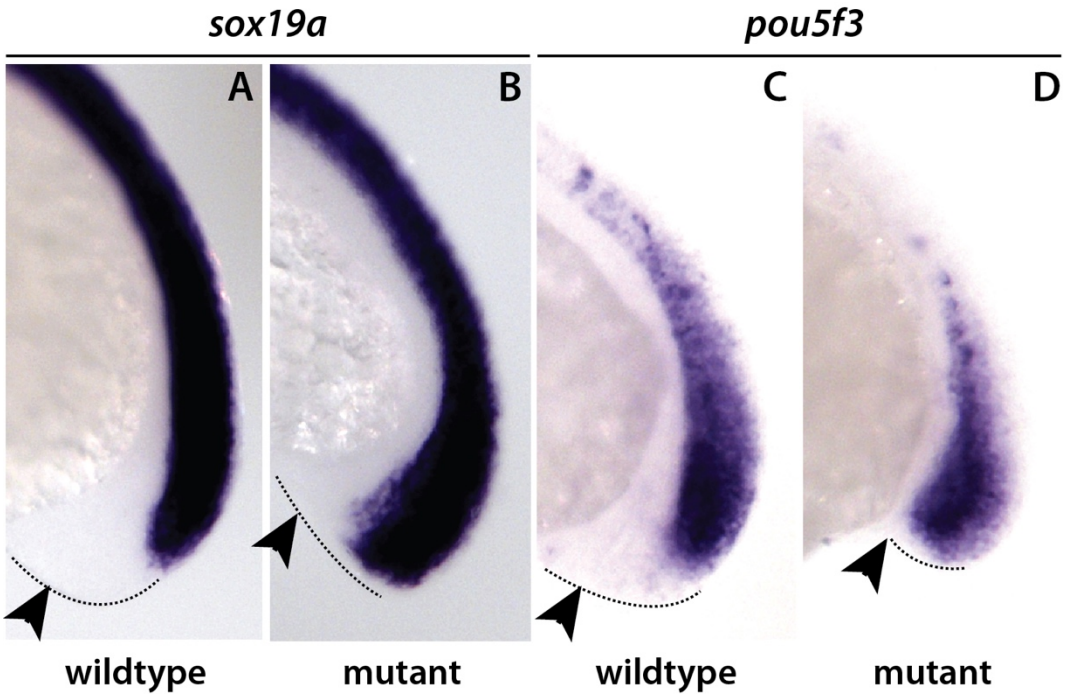

Figure S7 *sox19a and pou5f3* expression expands into the mesodermal progenitor region in *hoxa13;ntl^{cs}* mutants at 18.5° C. Refers to Figure 4.

A-D) In situ hybridization of 15s wildtype and *hoxa13;ntl^{cs}* embryos for the neural markers *sox19a* and *pou5f3*. As with *sox2*, expression expands into the prospective mesodermal territory in the *hoxa13;ntl^{cs}* mutants.

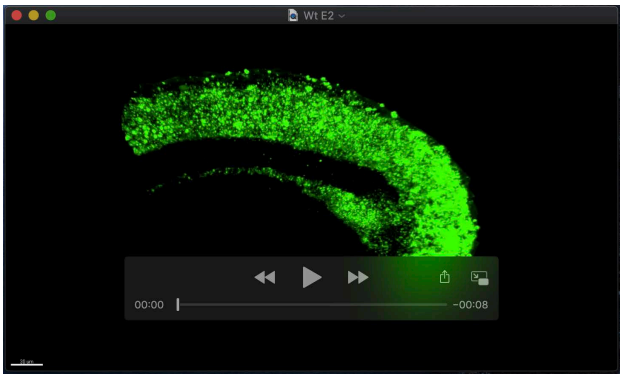

Movie 1. *sox2* expression in a wildtype embryo.
The same embryo as in Figure S6A-C.

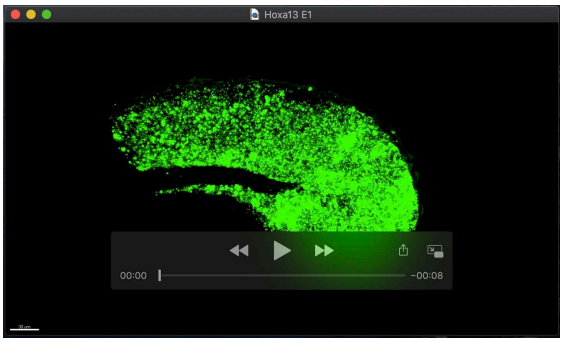

Movie 2. *sox2* expression in a *hoxa13;ntl*^{cs} mutant with a class 1 phenotype.
The same embryo as in Figure S6D-F.

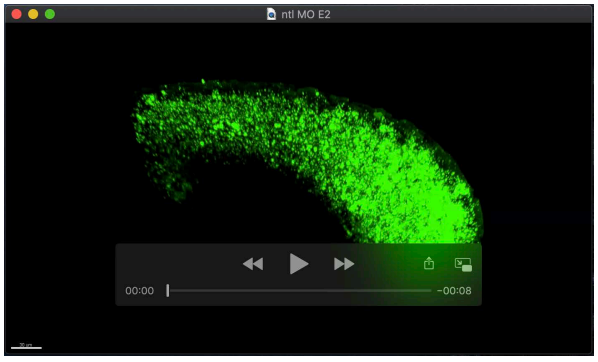

Movie 3. *sox2* expression in a *tbxta/ntl* morphant.
The same embryo as in Figure S6G-I.